

Curriculum-DPO++: Direct Preference Optimization via Data and Model Curricula for Text-to-Image Generation

Florinel-Alin Croitoru, Vlad Hondu, Radu Tudor Ionescu, *Member, IEEE*, Nicu Sebe, *Senior Member, IEEE*, and Mubarak Shah, *Fellow, IEEE*

Abstract—Direct Preference Optimization (DPO) has been proposed as an effective and efficient alternative to reinforcement learning from human feedback (RLHF). However, neither RLHF nor DPO take into account the fact that learning certain preferences is more difficult than learning other preferences, rendering the optimization process suboptimal. To address this gap in text-to-image generation, we recently proposed Curriculum-DPO, a method that organizes image pairs by difficulty, ensuring that increasingly challenging examples are progressively sampled and presented to a generative (diffusion or consistency) model. In this paper, we introduce Curriculum-DPO++, an enhanced method that combines the original data-level curriculum with a novel model-level curriculum. More precisely, we propose to dynamically increase the learning capacity of the denoising network as training advances. We implement this capacity increase via two mechanisms. First, we initialize the model with only a subset of the trainable layers used in the original Curriculum-DPO. As training progresses, we sequentially unfreeze layers until the configuration matches the full baseline architecture. Second, as the fine-tuning is based on Low-Rank Adaptation (LoRA), we implement a progressive schedule for the dimension of the low-rank matrices. Instead of maintaining a fixed capacity, we initialize the low-rank matrices with a dimension significantly smaller than that of the baseline. As training proceeds, we incrementally increase their rank, allowing the capacity to grow until it converges to the same rank value as in Curriculum-DPO. Furthermore, we propose an alternative ranking strategy to the one employed by Curriculum-DPO. While the original approach relies on external reward models to rank samples, we introduce an implicit scoring mechanism derived from prompt perturbations. This approach is particularly useful when auxiliary reward models are not available. Finally, we compare Curriculum-DPO++ against Curriculum-DPO and other state-of-the-art preference optimization approaches on nine benchmarks, outperforming the competing methods in terms of text alignment, aesthetics and human preference. Our code is available at <https://github.com/CroitoruAlin/Curriculum-DPO>.

Index Terms—diffusion models, consistency models, curriculum learning, preference optimization, preference alignment.

1 INTRODUCTION

DIFFUSION models [1]–[4] represent a family of generative models that gained significant traction in image generation tasks, largely due to their impressive generative capabilities. One of the tasks where these models excel is text-to-image generation [5]–[8], as they are capable of generating images that are both aesthetic and well aligned with the input text (prompt). However, state-of-the-art diffusion models that have been widely adopted by the community, e.g. Stable Diffusion [7], are typically heavy in terms of training (and even inference) time. To this end, several studies [9]–[12] proposed novel training methods to efficiently fine-tune pre-trained diffusion models. Some of these training frameworks [9], [11], [12] were originally introduced for Large Language Models (LLMs) [13]–[15], another family of models that are notoriously hard to train on a few GPUs [16], [17]. This is also the case of Direct Preference Optimization (DPO) [15], a method used to fine-tune LLMs, which was

originally proposed as an effective and efficient alternative to reinforcement learning from human feedback (RLHF) [13]. DPO bypasses the need to fit a reward model by harnessing a mapping between reward functions and optimal policies, which enables the direct optimization of the LLM to adhere to human preferences. DPO was later extended to diffusion models [12], showcasing similar benefits in image generation. Despite the significant benefits brought by Diffusion-DPO [12] and related methods [9]–[11], there are still observable gaps in terms of various factors, such as text alignment, aesthetics and human preference (see Figures 2, 9 and 10). Therefore, more advanced adaptation techniques are required to reduce these gaps.

One of the advancements that boosted the performance of Diffusion-DPO is our recent work, Curriculum-DPO [18], which was published at CVPR 2025. Curriculum-DPO stems from the fact that the preference pairs in Diffusion-DPO are randomly sampled during training, which is suboptimal. To mitigate this issue, Curriculum-DPO organizes the pairs according to their complexity with respect to the preference learning task, from easy to hard. The method comprises two stages. In the first stage, we employ a reward model to rank the images generated for each prompt according to their preference score. In the second stage, pairs of samples with different difficulty levels are created, leveraging the

• F.A. Croitoru, V. Hondu and R.T. Ionescu are with the Department of Computer Science, University of Bucharest, Bucharest, Romania. F.A. Croitoru and V. Hondu have contributed equally. R.T. Ionescu is the corresponding author.
E-mail: raducu.ionescu@gmail.com

• N. Sebe is with the University of Trento, Italy.

• M. Shah is with the Center for Research in Computer Vision (CRCV), University of Central Florida, Orlando, FL, US.

Manuscript received February 10, 2026; revised June 27, 2026.

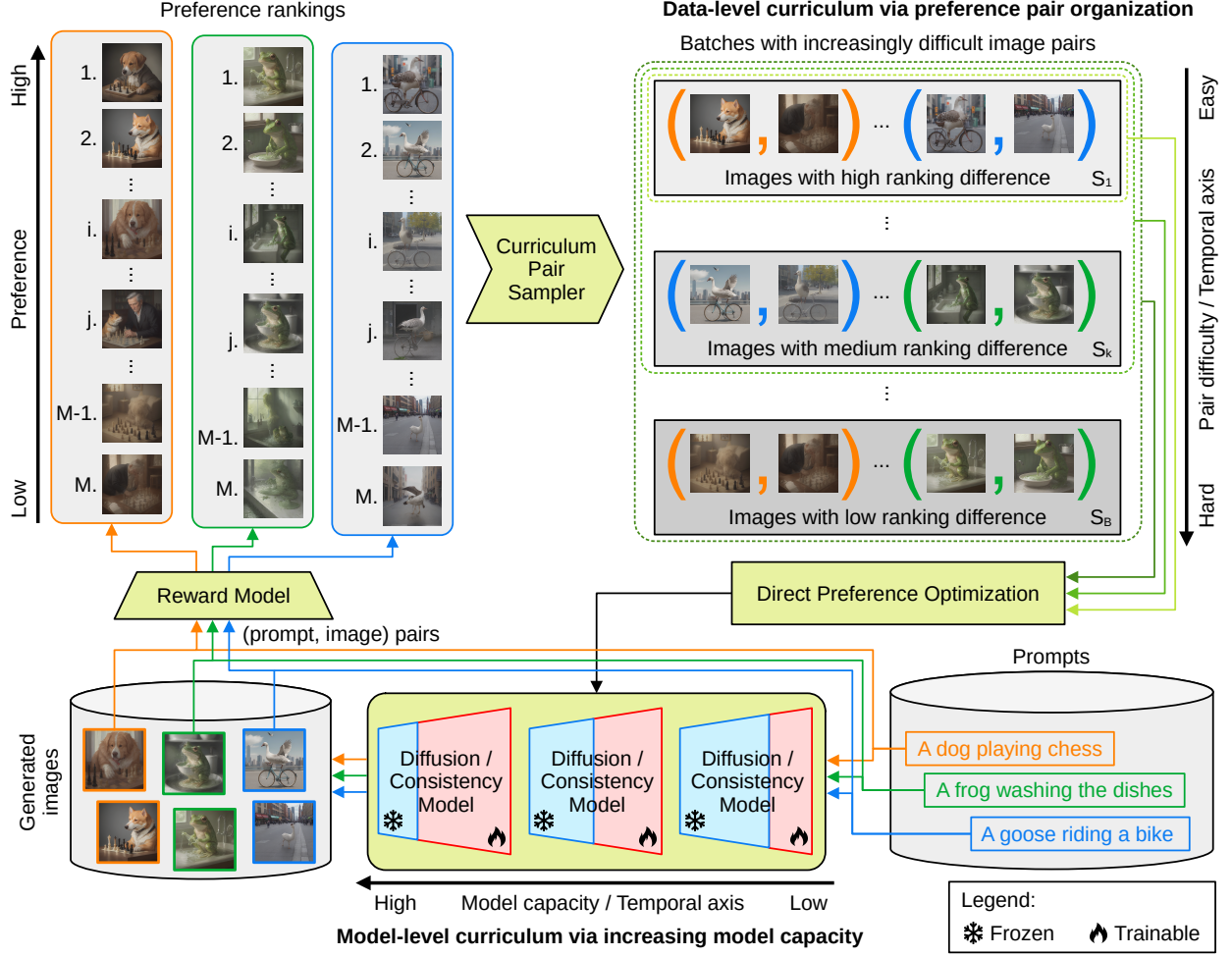


Fig. 1: An overview of Curriculum-DPO++. Images generated by a diffusion / consistency model and their prompts are passed through a reward model, obtaining a preference ranking for each prompt. Next, image pairs of various difficulty levels are generated and organized into batches, such that the initial batch contains easy pairs (with high difference in terms of preference scores) and subsequent batches contain increasingly difficult pairs (the difference in terms of preference is gradually decreased). The diffusion / consistency model is trained via Direct Preference Optimization (DPO) based on easy-to-hard data-level curriculum. Curriculum-DPO++ gracefully combines data-level and model-level curricula, increasing the learning capacity of the model to accommodate for the more complex examples gradually introduced during training. The learning capacity is expanded by unfreezing neural layers and increasing the rank of LoRA matrices. Best viewed in color.

rank difference between samples as a measure of difficulty. Samples that are far apart in the preference ranking are considered to form easy pairs. In contrast, samples that are close in the ranking form hard pairs, since choosing the preferred sample is less obvious. The sampled pairs are split into batches according to their difficulty level, allowing to organize the batches in a meaningful order, from easy to hard. This essentially generates an optimization process based on curriculum learning [19]. However, in the early training stages, a high capacity model may be prone to overfitting on easy examples, hurting performance and generalization. In this work, we propose to enhance Curriculum-DPO by synchronizing the original data-level curriculum with a novel model-level curriculum, as illustrated in Figure 1. We implement the model-level curriculum via two complementary mechanisms. The first mechanism guides the progressive expansion of trainable layers. We initialize the training with a minimal subset of neural components, comprising

only the bottleneck and the innermost downsampling and upsampling blocks. As we update the set of pairs in the data-level curriculum, we jointly expand the set of trainable layers by including additional outer downsampling and upsampling blocks. The second mechanism to realize the model-level curriculum operates on Low-Rank Adaptation (LoRA) matrices, since we run our fine-tuning using this procedure. We start with a small dimension for the low-rank matrices and, as we progress with the data-level curriculum, we also increase the dimension of the matrices. When we perform this dimension update, we copy the previously learned weights into the top-left part of the new larger matrices. The data-level and model-level curricula are gracefully integrated to adjust the learning capacity of the model to the current complexity of the training examples, resulting in a new framework, called Curriculum-DPO++.

As a secondary contribution, we introduce a reward-free alternative to the initial ranking stage of Curriculum-

DPO. Rather than relying on an external reward model, we construct synthetic preference pairs and derive their difficulty rankings directly through prompt embedding perturbations. Specifically, we apply varying degrees of masking to the text embeddings. The winning sample is universally defined as the image generated with a masking ratio of 0 (the clean prompt). The losing sample corresponds to the perturbed prompt. We then map the masking ratio to the curriculum difficulty. The pairs with a smaller masking ratio are regarded as difficult (since the degradation is subtle), while those with a higher masking ratio are considered easy (as the heavy masking renders the degradation obvious).

We carry out experiments across nine evaluation benchmarks to assess the effectiveness of our Curriculum-DPO enhancements in adapting text-to-image generative models to different reward models. We first tackle the text alignment task, employing the Sentence-BERT [20] similarity metric to evaluate the correspondence between the actual text prompt and the caption provided by the LLaVA model [21] for each generated image. Next, we focus on enhancing the visual aesthetics of the images, where we use the LAION Aesthetics Predictor [22] as the reward model. Finally, for the third task, we increase the human preference rate by employing HPSv2 [23] as the reward model. Each of the three tasks is studied on three distinct datasets. The quantitative and qualitative results on all datasets show that Curriculum-DPO++ consistently outperforms the original Curriculum-DPO and other state-of-the-art fine-tuning strategies, such as Diffusion-DPO [12], [15] and Denoising Diffusion Policy Optimization (DDPO) [9].

In summary, our contribution is fivefold:

- We provide an extended presentation of Curriculum-DPO [18], a training regime for diffusion and consistency models, which enhances DPO via data-level curriculum learning.
- We provide an extended presentation of our DPO adaptation for consistency models, termed Consistency-DPO [18].
- We introduce a novel model-level curriculum framework that enhances Curriculum-DPO by increasing its learning capacity along with the complexity of the preference pairs, resulting in a new framework called Curriculum-DPO++.
- We propose a reward-free alternative to Curriculum-DPO.
- We demonstrate the superiority of Curriculum-DPO++ over Curriculum-DPO and other state-of-the-art training alternatives on nine evaluation benchmarks.

2 RELATED WORK

Diffusion models. In recent years, diffusion models have gained a lot of traction [1]–[4], [7], [24], becoming one of the state-of-the-art generative methods, due to their capability to synthesize diverse images with high-fidelity, greatly surpassing Generative Adversarial Networks (GANs) [25], the prior leading approach. Given their wide adoption, significant efforts were undertaken to improve the capability of diffusion models across multiple dimensions. One dimension regards the introduction of conditioning mechanisms for different

modalities, *e.g.* text prompts [5], [6], [26], [27], images [28]–[30] or class labels [31]–[33]. Another dimension is finding new downstream applications, *e.g.* inpainting [34], [35], super-resolution [36], [37], medical imaging [38], [39], etc. Despite the important research endeavors of both academia and industry, the main limitation of diffusion models is represented by their slow inference speed. More precisely, diffusion models need to execute many sequential denoising operations, which heavily slows down the sampling time. Consequently, considerable attention has been directed towards the sampling process through improved scheduling strategies [40]–[42]. Building towards the goal of reducing inference time, Song *et al.* [43] proposed consistency models, a new family of diffusion models requiring less denoising steps. Consistency models were further developed in follow-up studies, *e.g.* [44], [45]. To the best of our knowledge, DPO was not studied in conjunction with consistency models before our preliminary work [18]. In this work, we describe in detail how DPO can be adapted to consistency models.

Controllable generation for diffusion models. Guiding the image generation process in diffusion models using various signals has been a major research focus. The initial approaches leveraged the gradients of a classifier to steer synthesis [24], [25], [31]. Ho *et al.* [46] later refined by introducing classifier-free guidance for conditional generation.

Building upon the same line of work, Zhang *et al.* [47] proposed ControlNet, a framework that enables an additional control input (mostly for the structure) to any text-to-image diffusion model, without retraining the original model. Their method involves several architectural modifications. While keeping the original U-Net intact, trainable copies of the encoder blocks and middle blocks are created for the control input. These are further integrated with the original decoder blocks with zero-convolutional layers.

Due to their great success, the recent advances in LLMs have also been quickly adopted in the development of diffusion models. Hu *et al.* [14] introduced Low-Rank Adaptation (LoRA), a parameter-efficient fine-tuning methodology for LLMs through low-rank matrix factorization of selected transformer layers, while preserving the pre-trained parameters. LoRA brings improved performance with reduced memory overhead. Luo *et al.* [11] employed LoRA [14] on consistency models, demonstrating better results, while requiring less memory.

A fundamental limitation of standard LLM training objectives is that they fail to adequately capture human preferences, while commonly-used metrics (*e.g.* BLEU [48]) are imperfect proxies. This motivated the switch from standard supervised training to reinforcement learning [49]–[51]. Lee *et al.* [52] demonstrated improved text-image alignment by training a reward model on data labeled from human feedback. The reward model is further used to guide the fine-tuning of a text-to-image diffusion model. Policy gradients methods, instrumental for the success of LLMs, have also been integrated into diffusion models. While Fan *et al.* [10] demonstrated that such an algorithm leads to an improved text-image alignment, Black *et al.* [9] applied their preference optimization method to enhance multiple aspects of synthesis: compressibility, aesthetics, as well as prompt alignment. More recently, Rafailov *et al.* [15] introduced Direct Preference Optimization (DPO), which eliminates the

intermediate reward model and enables fine-tuning LLMs directly on the preference, by providing a pair of winning and losing samples. DPO demonstrates superior performance than several Proximal Policy Optimization methods [51], [53], [54]. Wallace *et al.* [12] integrated DPO into diffusion models through a custom objective function and training procedure, reporting improvements on subjective metrics, such as visual aesthetics or prompt alignment. To the best of our knowledge, curriculum learning was first applied in conjunction with controllable generation methods for diffusion models in our preliminary study [18]. In this study, we introduce an enhanced version of Curriculum-DPO [18], which integrates data and model curricula in a meaningful way.

Curriculum learning. Inspired by how people learn, Bengio *et al.* [19] proposed *curriculum learning*, a learning paradigm to train neural networks starting with an easier task, and then progressively increasing its difficulty. Despite the early introduction of curriculum learning more than a decade ago, it remains an active research direction [55]–[57], usually being integrated into the learning process of numerous neural models. Soviany *et al.* [55] established four categories of curriculum learning, according to the level of operation: data, model, task, and optimization objective. Among these, data-level and model-level curricula are more popular, essentially because of their wider applicability across tasks. Data-level curriculum studies how organizing samples based on their complexity influences the training process [19], [58]–[63]. Model-level curriculum focuses on increasing the learning power of the model during training [64]–[68], essentially eliminating the need to assess sample difficulty. A wide number of works in computer vision applied various forms curriculum learning [55], [56]. Nevertheless, its application in image generation has been rather limited, being mainly focused on GANs [64], [69]–[71]. Given the recent surge of interest in diffusion models, easy-to-hard curriculum learning has been explored for this class of generative models [72]–[74]. Kim *et al.* [72] and Xu *et al.* [73] advocated to start the training from higher diffusion timesteps (with more noise) and progress to lower timesteps (with less noise). Their methods are completely different from our work, as we concentrate on the difficulty with respect to the preference scores rather than the noise levels. Building upon our previous work [18], Na *et al.* [74] proposed a fine-tuning strategy based on Curriculum-DPO for diffusion models. While very similar to our method, the main distinction is that their winning samples are based on real images, except for the first stage. Moreover, their training stages (easy, intermediate and hard) are related to the provenance of the winning samples. To the best of our knowledge, we are the first to combine data-level and model-level curricula by adjusting the learning capacity of the model with respect to the difficulty of the training samples. As the difficulty grows from easy to hard, the learning capacity is proportionally increased, avoiding overfitting on easy examples in the early training stages.

3 METHOD

Before diving into the details behind Curriculum-DPO++, we briefly discuss preliminaries regarding diffusion models, consistency models, DPO, and Diffusion-DPO. For a more

detailed introduction of these concepts, please refer to Appendix 6.1.

3.1 Preliminaries

Diffusion models. Diffusion models are probabilistic generative models that reconstruct data samples, $x_0 \sim p(x_0)$, from Gaussian noise. The training consists of a forward diffusion process that perturbs each data sample into a noisy version x_t via a transition $x_t = \alpha_t x_0 + \sigma_t \epsilon$, where $\epsilon \sim \mathcal{N}(0, \mathbf{I})$ and $\{\alpha_t, \sigma_t\}_{t=1}^T$ defines the variance schedule. Learning is formulated as a noise-prediction task. We optimize a neural network $\epsilon_\theta(x_t, t)$, with parameters θ , to approximate the underlying noise component ϵ using the standard mean squared error loss:

$$\mathcal{L}_{\text{simple}} = \mathbb{E}_{t \sim \mathcal{U}(1, T), \epsilon \sim \mathcal{N}(0, \mathbf{I}), x_0 \sim p(x_0)} \|\epsilon_t - \epsilon_\theta(x_t, t)\|_2^2. \quad (1)$$

Sampling is achieved by reversing this trajectory. We start with pure noise $x_T \sim \mathcal{N}(0, \mathbf{I})$ and iteratively refine the image using ϵ_θ . At each step t , we subtract the predicted noise from the image, pushing the image towards the original data manifold.

Consistency models. Consistency models [43]–[45] leverage the deterministic Probability Flow ODE (PF-ODE) formulation of diffusion [24]. They are trained to map arbitrary states x_t on the solution trajectory directly to the origin x_0 . This property is induced via a self-consistency constraint, requiring the model output to be identical for two points belonging to the same ODE trajectory. The training objective minimizes the distance between the current model output and a target estimated from the previous step:

$$\mathcal{L}_{\text{CD}}(\phi) = d(f_\phi(x_{t_{n+1}}, t_{n+1}), f_{\phi^-}(\hat{x}_{t_n}^\theta, t_n)), \quad (2)$$

where $\hat{x}_{t_n}^\theta$ is a one-step estimate of the next state derived by a pre-trained frozen diffusion model, ϵ_θ , using a numerical ODE solver. The target network utilizes exponential moving average (EMA) weights ϕ^- to stabilize training, and N represents the discretization of the time interval $[0, T]$, $n \sim \mathcal{U}(1, N)$, ϕ are the trainable parameters of the consistency model, and d is a distance metric.

Direct Preference Optimization (DPO). To align a generative model with human preferences, Rafailov *et al.* [15] introduced DPO. This approach fine-tunes models directly on preference pairs (x_0^w, x_0^l, c) , where c represents the context, and x_0^w is the preferred (winning) generated output over x_0^l (losing). The method implicitly optimizes a reward function by ensuring the model prefers x_0^w , while remaining close to the original reference distribution, $p_{\text{ref}}(x_0|c)$. The training objective minimizes the negative log-likelihood of the preference data using a ratio-based formulation:

$$\mathcal{L}_{\text{DPO}}(\theta) = -\mathbb{E}_{x_0^w, x_0^l, c} \left[\log \sigma \left(\beta \left(\log \frac{p_\theta(x_0^w|c)}{p_{\text{ref}}(x_0^w|c)} - \log \frac{p_\theta(x_0^l|c)}{p_{\text{ref}}(x_0^l|c)} \right) \right) \right], \quad (3)$$

where the term inside the sigmoid σ represents the difference in implicit rewards assigned to the winning and losing samples. The coefficient β controls how strictly the optimization is anchored to the reference model p_{ref} . The intuition behind \mathcal{L}_{DPO} becomes clearer when analyzing how the parameters are updated during training. If we define the implicit reward for a sample as $\hat{r}_\theta(x_0, c) = \beta \cdot \log \frac{p_\theta(x_0|c)}{p_{\text{ref}}(x_0|c)}$, the derivative

of the loss function with respect to the parameters θ of the model is the following:

$$\frac{\partial \mathcal{L}_{\text{DPO}}(\theta)}{\partial \theta} = -\beta \mathbb{E}_{x_0^w, x_0^l, c} \left[\sigma \left(\hat{r}_\theta(x_0^l, c) - \hat{r}_\theta(x_0^w, c) \right) \cdot \left(\frac{\partial \log p_\theta(x_0^w | c)}{\partial \theta} - \frac{\partial \log p_\theta(x_0^l | c)}{\partial \theta} \right) \right]. \quad (4)$$

Eq. (4) has two key properties. First, the gradient direction acts to increase the probability of the preferred output x_0^w , while suppressing the disfavored x_0^l . Second, the magnitude of the update is dynamically scaled by the sigmoid term $\sigma(\hat{r}_\theta(x_0^l, c) - \hat{r}_\theta(x_0^w, c))$, acting like a weighting factor. It approaches 1 when the model incorrectly assigns a higher reward to the losing sample, making the update strong, and vanishes towards 0 when the model correctly ranks the two examples.

Diffusion-DPO. To apply DPO to the continuous domain of diffusion, Wallace *et al.* [12] replaced the log-probability terms with MSE objectives. The resulting loss penalizes the model if the denoising error on the preferred sample x_t^w is not significantly lower than the error on the rejected sample x_t^l , relative to the reference model. The objective is defined as:

$$\mathcal{L}_{\text{Diff-DPO}}(\theta) = -\mathbb{E}_{x_t^w, x_t^l, c} \left[\log \sigma \left(-\beta \cdot T \left(\|\epsilon^w - \epsilon_\theta^w(x_t^w, t, c)\|_2^2 - \|\epsilon^w - \epsilon_{\text{ref}}^w(x_t^w, t, c)\|_2^2 - \|\epsilon^l - \epsilon_\theta^l(x_t^l, t, c)\|_2^2 + \|\epsilon^l - \epsilon_{\text{ref}}^l(x_t^l, t, c)\|_2^2 \right) \right) \right], \quad (5)$$

where x_t^w and x_t^l represent the diffusion samples at timestep t , obtained by adding noise to the original pair (x_0^w, x_0^l) .

3.2 Consistency-DPO

We extend the Diffusion-DPO formulation of Wallace *et al.* [12] to consistency models. Instead of using the denoising error, we leverage the consistency distillation loss in Eq. (2) as a proxy for sample quality. The core principle of our approach is to optimize the parameters of the model such that the consistency mapping error is minimized for preferred examples $x_{t_n}^w$ compared with dispreferred examples $x_{t_n}^l$. Thus, we define the training objective as:

$$\mathcal{L}_{\text{Con-DPO}}(\phi) = -\mathbb{E}_{x_{t_{n+1}}^w, x_{t_{n+1}}^l, c} \left[\log \sigma \left(-\beta \left(d^w(x_{t_{n+1}}^w, \hat{x}_{t_n}^{w,\theta}, \phi) - d^l(x_{t_{n+1}}^l, \hat{x}_{t_n}^{l,\theta}, \phi) \right) \right) \right], \quad (6)$$

where, for $* \in \{w, l\}$, the distance d^* is defined as:

$$d^* = d(f_\phi(x_{t_{n+1}}^*, t_{n+1}, c), f_{\text{ref}}(\hat{x}_{t_n}^{*,\theta}, t_n, c)) - d(f_{\text{ref}}(x_{t_{n+1}}^*, t_{n+1}, c), f_{\text{ref}}(\hat{x}_{t_n}^{*,\theta}, t_n, c)). \quad (7)$$

The input $x_{t_{n+1}}^*$ is derived from x_0^* (where $* \in \{w, l\}$) via the standard forward process. The target estimate $\hat{x}_{t_n}^{*,\theta}$ is computed by advancing $x_{t_{n+1}}^*$ one step along the PF-ODE using a pre-trained diffusion model θ . The optimization is based on the distance metric d and sigmoid σ , with indices $n \sim \mathcal{U}(1, N)$ spanning the discretization of the time interval. The active parameters of the consistency model are represented by ϕ . We diverge from standard practice by excluding the parameter running average (ϕ^-), as the frozen reference consistency model f_{ref} already has the self-consistency property.

To validate that Consistency-DPO shares the optimization dynamics of the original DPO (Eq. (3)) and Diffusion-DPO (Eq. (5)), we further examine the gradient of the loss with respect to the parameters ϕ :

$$\frac{\partial \mathcal{L}_{\text{Con-DPO}}}{\partial \phi} = \beta \mathbb{E}_{x_{t_{n+1}}^w, x_{t_{n+1}}^l, c} \left[\sigma \left(\beta \left(d^w - d^l \right) \right) \left(\frac{\partial d^w}{\partial \phi} - \frac{\partial d^l}{\partial \phi} \right) \right]. \quad (8)$$

Eq. (8) reduces the consistency metric d^w for the favored samples, while increasing d^l for the less preferred examples. The strength of this correction is dynamically weighted by $\sigma(d^w - d^l)$, which approaches 1 when f_ϕ exhibits a weaker preference for x^w compared with f_{ref} , ensuring that the model learns primarily from misranked pairs.

3.3 Curriculum-DPO

In our preliminary work [18], we challenge the assumption that all preference pairs are equally informative at all stages of training. We observe that preference is hierarchical, *i.e.* some choices are obvious, for example broken versus coherent images, while others are subtle. To exploit this, we implement a coarse-to-fine learning process. The model is initially trained on pairs with high-level semantic discrepancies, allowing it to rapidly grasp fundamental preference directions. As training advances, the curriculum shifts toward pairs requiring fine-grained discrimination. Formally, we propose a curriculum guided by the reward model $r_\varphi(x_0, c)$, which serves as a proxy for establishing ground-truth rankings. By leveraging the score differential between the winner and loser in a pair (x_0^w, x_0^l) , we can estimate the distinctiveness of the preference signal. Wide gaps in scoring suggest easy pairs, where the superior sample is visually distinct due to coarse-level factors. Narrow gaps indicate hard pairs, where the preference relies on subtle details. We also use a lower-bound cutoff on this difference. This ensures the model ignores pairs where the preference decision is ambiguous, thereby mitigating the risk of fitting to the reward model's biases, rather than true signal.

In Algorithm 1, we outline the Curriculum-DPO++ procedure. By ignoring steps 6-7 and 12-19, we obtain the original Curriculum-DPO. Initially, M samples are sorted by a reward score r_φ (step 1). Next, we partition the set of valid preference pairs into B difficulty levels (subsets S_k), determined by the rank difference between paired samples bounded by $[L_k, R_k]$. Training proceeds progressively (steps 11-27). At each stage k , the corresponding subset S_k is merged into the active training set P , followed by H_k optimization steps. The process starts with S_1 , representing the pairs with the most obvious preference signals. The last part of the algorithm (steps 21-27) comprises steps specific to Consistency-DPO. The corresponding derivation for Diffusion-DPO is available in Appendix 6.2.

3.4 Curriculum-DPO++

When preference patterns are evident, a shallow model should be sufficient to distinguish between winning and losing samples. As the complexity of training samples increases during training, the learning capacity of the model must expand to cope with the harder preference learning task. However, using a model with fixed learning capacity is suboptimal, since a high-capacity model can overfit on

Algorithm 1: Curriculum-DPO++ (for consistency models)

Input: $\{(x_{0,i}, c)\}_{i=1}^M$ - the training samples, $r_\phi(x_0, c)$ - the reward model which can be conditioned on c , B - the number of batches for splitting the set of pairs, θ - the parameters of a pre-trained diffusion model, α_t, σ_t - the parameters of the noise schedule, T - the last diffusion timestep, N - the discretization length of the interval $[0, T]$, β - DPO hyperparameter to control the divergence from the initial pre-trained state, σ - the sigmoid function, d^* - as defined in Eq. (7), η - the learning rate, $\{H_k\}_{k=1}^B$ - the number of training iterations after including the k -th batch, $\{G_k\}_{k=1}^B$ - the trainable layers after including the k -th batch, ϕ - the pre-trained weights of the reference model, $\mathbf{r}_{\text{start}}$ - the rank of the LoRA adaptation matrices at the start of the training, \mathbf{r}_{end} - the rank of the LoRA adaptation matrices at the end of the training, δ - the rank update rate.

Output: ϕ - the trained weights of the consistency model.

- 1 $\hat{X} \leftarrow \{(x_{0,i}, c) | r_\phi(x_{0,i}, c) \leq r_\phi(x_{0,i-1}, c), i = \{2, 3, \dots, M\}\}$; \triangleleft sort the samples in descending order of the rewards
- 2 $S \leftarrow \{(x_{0,i}, x_{0,j}, c) | i, j \in \{1, \dots, M\}; i < j; x_{0,i}, x_{0,j} \in \hat{X}, r_\phi(x_{0,i}, c) > r_\phi(x_{0,j}, c)\}$; \triangleleft create pairs of examples using the order from \hat{X}
- 3 $L_k \leftarrow \left\{ \frac{(M-1) \cdot (B-k)}{B} \right\}_{k=1}^B$; \triangleleft the minimum preference limits of the batches
- 4 $R_k \leftarrow \left\{ \frac{(M-1) \cdot (B-(k-1))}{B} \right\}_{k=1}^B$; \triangleleft the maximum preference limits of the batches
- 5 $S_k \leftarrow \{(x_0^w, x_0^l, c) | (x_0^w, x_0^l) = (x_{0,i}, x_{0,j}), L_k < j - i \leq R_k; (x_{0,i}, x_{0,j}, c) \in S\}_{k=1}^B$; \triangleleft the batches of increasingly difficult pairs
- 6 $\mathbf{r} \leftarrow \{\mathbf{r}_k | k \in \{1, \dots, B\}, \mathbf{r}_1 = \mathbf{r}_{\text{start}}, \mathbf{r}_{k+1} = \min(\mathbf{r}_{\text{end}}, \mathbf{r}_k \cdot \delta)\}$; \triangleleft the ranks of the low-rank matrices in LoRA
- 7 $\text{LoRA}_k = \{(A_i^{\mathbf{r}_k}, C_i^{\mathbf{r}_k}) | i \in G_k, A_i^{\mathbf{r}_k} \sim \mathcal{N}(0, \sigma), C_i^{\mathbf{r}_k} = \mathbf{0}_{m \times \mathbf{r}_k}\}_{k=1}^B$; \triangleleft initialization of LoRA matrices
- 8 $P \leftarrow \emptyset$; \triangleleft current training set
- 9 $G \leftarrow \emptyset$; \triangleleft current trainable layers
- 10 **foreach** $k \in \{1, \dots, B\}$ **do**
 - 11 $P \leftarrow P \cup S_k$; \triangleleft include a new batch in the training
 - 12 $G^{\text{new}} \leftarrow \text{LoRA}_k$; \triangleleft include a new set of trainable layers
 - 13 **foreach** $(A_i^{\mathbf{r}_k}, C_i^{\mathbf{r}_k}) \in G^{\text{new}}$ **do**
 - 14 **if** $i < |G|$ **then**
 - 15 $\quad //$ transfer the previously learned weights to the new LoRA matrices
 - 16 $\quad A_i^{\mathbf{r}_{k-1}}, C_i^{\mathbf{r}_{k-1}} \leftarrow G_i$
 - 17 $\quad A_i^{\mathbf{r}_k}[:, \mathbf{r}_{k-1}, :] \leftarrow A_i^{\mathbf{r}_{k-1}}$
 - 18 $\quad C_i^{\mathbf{r}_k}[:, :, \mathbf{r}_{k-1}] \leftarrow C_i^{\mathbf{r}_{k-1}}$
 - 19 $G \leftarrow G^{\text{new}}$
 - 20 **foreach** $i \in \{1, \dots, H_k\}$ **do**
 - 21 $(x_0^w, x_0^l, c) \sim \mathcal{U}(P); n \sim \mathcal{U}[1, N-1]; \epsilon \sim \mathcal{N}(0, \mathbf{I})$
 - 22 $x_{t_{n+1}}^w \leftarrow \alpha_{t_{n+1}} x_0^w + \sigma_{t_{n+1}} \epsilon$; \triangleleft forward process
 - 23 $x_{t_{n+1}}^l \leftarrow \alpha_{t_{n+1}} x_0^l + \sigma_{t_{n+1}} \epsilon$; \triangleleft forward process
 - 24 $\hat{x}_{t_n}^{w, \theta} \leftarrow \text{ODESolver}(x_{t_{n+1}}^w, \theta, \alpha_{t_{n+1}}, \sigma_{t_{n+1}})$; \triangleleft one denoising step
 - 25 $\hat{x}_{t_n}^{l, \theta} \leftarrow \text{ODESolver}(x_{t_{n+1}}^l, \theta, \alpha_{t_{n+1}}, \sigma_{t_{n+1}})$; \triangleleft one denoising step
 - 26 $\mathcal{L}_{\text{Con-DPO}}(\phi, G) \leftarrow -\log \sigma(-\beta(d^w(x_{t_{n+1}}^w, \hat{x}_{t_n}^{w, \theta}, \phi, G) - d^l(x_{t_{n+1}}^l, \hat{x}_{t_n}^{l, \theta}, \phi, G)))$; \triangleleft DPO loss, as in Eq. (6)
 - 27 $G \leftarrow G - \eta \frac{\partial \mathcal{L}_{\text{Con-DPO}}}{\partial G}$; \triangleleft update the weights
 - 28 $\phi \leftarrow \phi + G$; \triangleleft store the LoRA weights into the original model
 - 29 **return** ϕ

easy examples, while a low-capacity model might underfit on hard examples. To address the misalignment between model capacity and task complexity, we complement our data-level curriculum with a new model-level curriculum that progressively scales the complexity of the network along with the difficulty of the preference pairs. Since the fine-tuning is based on LoRA [14], we propose to grow the learning capacity of the model during training via dynamically increasing (i) the rank of the low-rank matrices and (ii) the number of trainable layers.

In Algorithm 1, we detail the Curriculum-DPO++ training process for consistency models, which includes the process

of scaling the learning capacity of the model when introducing more complex preference pairs. We establish two schedules synchronized with the introduction of each data-level curriculum batch $S_k, \forall k = \{1, \dots, B\}$. First, we define the layer schedule $\{G_k\}_{k=1}^B$, where G_k denotes the set of active trainable layers for the k -th data batch, such that G_k contains more and more layers as k grows. In practice, at each iteration, we add one upsampling and one downsampling block to the new set of trainable layers. Second, we govern the model capacity via a rank schedule for the LoRA matrices. The standard LoRA approximates the weight updates via

two fixed-size low-rank matrices, $C \in \mathbb{R}^{m \times r}$ and $A \in \mathbb{R}^{r \times h}$, where h is the size of the input features, m is the size of the output features, and $r \ll \min(m, h)$ determines the rank of the two matrices. In our algorithm, the rank r_k is not fixed during training, as it changes according to the hyperparameters r_{start} , r_{end} , and the growth rate δ , as formalized in step 6 of Algorithm 1. However, we emphasize that the chosen values still respect the low-rank property $r_k \ll \min(m, h)$. In step 7, we initialize all the matrices that are to be used throughout the training, but in practice, we can initialize these matrices exactly when we need them. Before entering the training loop on curriculum batch S_k , we establish the trainable layers in step 12 of the algorithm. If $k > 1$, we transfer the weights from the previously learned LoRA matrices to the new ones in steps 13-18. In step 28, the final LoRA weights are integrated into the pre-trained consistency model ϕ , leading to a preference-tuned version of the respective model.

3.5 Reward-Model-Free Curriculum

As an orthogonal contribution, we introduce a curriculum-based training methodology that eliminates the need for an explicit reward model. Instead of assigning external scores to each image, we induce implicit preference signals by perturbing the prompt embeddings used for image generation. Specifically, with the text alignment task in mind, we apply a masking operation on the prompt embedding, *i.e.* zero masking. Higher masking ratios disrupt the semantic information provided to the generator, resulting in images that exhibit weaker adherence to the input prompt, and sometimes, reduced synthesis quality. With these degraded samples, we can naturally form winning-losing pairs for DPO fine-tuning, where unmasked prompt embeddings serve to generate preferred outcomes.

To incorporate a curriculum strategy, we vary the masking ratio from 0.9 to 0.1. At the start of training, winning samples correspond to images generated from unmasked prompts, while losing samples are drawn from prompts with a masking ratio of 0.9. Over time, we progressively introduce losing samples with smaller masking ratios, enabling the model to learn increasingly subtle distinctions in text-image alignment. It is important to note that we always use unmasked examples as winning samples. Therefore, the easy-to-hard curriculum is created by decreasing the masking ratio from 0.9 to 0.1 for the losing examples.

4 EXPERIMENTS

Datasets. We conduct experiments across three datasets, denoted as D_1 , D_2 and D_3 . We adopt the data generation methodology of Black *et al.* [9] to construct the first dataset (D_1). For text alignment and human preference, we utilize Subject-Verb-Object (SVO) prompts (*e.g.* “a dog washing the dishes”) derived from a combination of 45 animal classes and 3 activity types. For the aesthetics task, we use the template “a photo of <an object>”, sampling from the same 45 animal classes. By generating 500 images per prompt, we obtain 67,500 training and 6,750 evaluation pairs for the alignment and preference tasks, while the aesthetics task comprises 22,500 training and 2,250 evaluation pairs.

Dataset D_2 is based on DrawBench [8]. By generating 500 images for each of its 200 prompts, we construct a set

of 100,000 pairs for training. For evaluation, we generate 50 images per prompt, resulting in a total of 10,000 images.

Dataset D_3 consists of 150,000 pairs from Pick-a-Pic [75], a dataset where images are already provided. For Pick-a-Pic, we evaluate on 500 official test prompts.

Generative models. Our experiments leverage two pre-trained generative models, namely the Stable Diffusion (SD) model [7] and the Latent Consistency Model (LCM) [44]. The LCM checkpoint is derived via consistency distillation from SD v1.5. For SD, we generate images of 256×256 pixels using 50 DDIM steps, whereas for LCM, we generate image at a resolution of 768×768 pixels using 8 steps of Multistep Latent Consistency Sampling [44].

Reward models. Following the reward modeling protocol of Black *et al.* [9], we employ three metrics to guide and evaluate our models. To measure text alignment, we compute the cosine similarity between Sentence-BERT [20] embeddings of the original prompt and a caption generated by LLaVA [21]. For visual appeal, we utilize the LAION Aesthetics Predictor [22], a linear model based on CLIP [76] representations. Finally, human preference is estimated using HPSv2 [23], a CLIP model fine-tuned on human-ranked image pairs. Crucially, DPO, DDPO, Curriculum-DPO and Curriculum-DPO++ utilize identical reward models to ensure a fair and consistent comparison.

Competing methods. We compare Curriculum-DPO++ with the original Curriculum-DPO [18], as well as established fine-tuning techniques, including Direct Preference Optimization (DPO) [12], [15] and Denoising Diffusion Policy Optimization (DDPO) [9]. Additionally, we include the pre-trained base models (LCM and SD) as reference points.

Training setup. We execute all experiments on a single H100 GPU, training for 10,000 iterations with a batch size of 16 and two steps of gradient accumulation. Computationally, LCM experiments require approximately 64GB of VRAM and 48 hours to complete, whereas SD experiments utilize 36GB of VRAM and finish in approximately 24 hours.

We optimize using AdamW with a fixed learning rate of $5 \cdot 10^{-5}$. LoRA is applied in all cases, configured with rank and scale values of $r=64$ and $\alpha=64$ for LCM, and $r=8$ and $\alpha=8$ for SD, respectively. For our model-level curriculum, we choose the hyperparameters for LCM as follows: $r_{\text{start}}=4$, $r_{\text{end}}=64$ and $\delta=2$. For SD, we use the following values: $r_{\text{start}}=6$, $r_{\text{end}}=16$ and $\delta=2$. The layer schedule $\{G_k\}_{k=1}^B$ is implemented via a progressive growth strategy. Training starts with the middle block and the innermost upsampling and downsampling layers. At each subsequent stage k , the set of trainable layers expands by incorporating an additional symmetrical pair of downsampling and upsampling blocks. For the reward-model-free experiments, we begin with losing samples having a 0.9 masking ratio, and decrease it by 0.1 every 1,000 steps.

We set $\beta=5000$ for Diffusion-DPO [12], and $\beta=200$ for Consistency-DPO. The number of curriculum batches is set to $B=5$ for both models. We define the iteration schedule as $H_i = K = 400$ for the initial batches $i \in \{1, \dots, 4\}$. The final batch consumes the remaining budget ($H_5 = 10,000 - 4 \cdot K$), ensuring that the total number of iterations matches the 10,000 iterations of the baselines, for a fair comparison. Regarding sampling, we select image pairs based on the magnitude of their preference score difference rather than

Dataset	Fine-Tuning Strategy	LCM			SD		
		Text Alignment	Aesthetics	Human Preference	Text Alignment	Aesthetics	Human Preference
D_1 [9]	-	0.7243 ± 0.0048	6.0490 ± 0.0162	0.2912 ± 0.0021	0.6804 ± 0.0052	5.5152 ± 0.0166	0.2784 ± 0.0015
	DDPO [9]	0.7490 ± 0.0036	6.3730 ± 0.0130	0.2952 ± 0.0011	0.7629 ± 0.0040	5.8183 ± 0.0129	0.2854 ± 0.0012
	DPO [12]	0.7502 ± 0.0045	6.4741 ± 0.0095	0.2990 ± 0.0010	0.7614 ± 0.0049	5.7146 ± 0.0162	0.2827 ± 0.0008
	Curriculum-DPO [18]	0.7548 ± 0.0041	6.6417 ± 0.0083	0.3237 ± 0.0012	0.7703 ± 0.0036	5.8232 ± 0.0197	0.2856 ± 0.0015
	Curriculum-DPO++	0.7603 ± 0.0013	6.7065 ± 0.0080	0.3241 ± 0.0012	0.7744 ± 0.0037	5.8342 ± 0.0125	0.3325 ± 0.0008
D_2 [8]	-	0.5602 ± 0.0032	5.8038 ± 0.0139	0.2610 ± 0.0016	0.5997 ± 0.0067	5.4292 ± 0.0181	0.2646 ± 0.0011
	DDPO [9]	0.5721 ± 0.0043	6.0121 ± 0.0127	0.2803 ± 0.0019	0.6024 ± 0.0055	5.6748 ± 0.0162	0.2673 ± 0.0025
	DPO [12]	0.5720 ± 0.0040	6.0430 ± 0.0113	0.2814 ± 0.0023	0.6075 ± 0.0057	5.6205 ± 0.0152	0.2672 ± 0.0013
	Curriculum-DPO [18]	0.5812 ± 0.0038	6.1829 ± 0.0128	0.2851 ± 0.0017	0.6234 ± 0.0050	5.7060 ± 0.0177	0.2681 ± 0.0019
	Curriculum-DPO++	0.5858 ± 0.0025	6.3626 ± 0.0622	0.2903 ± 0.0018	0.6247 ± 0.0014	5.8890 ± 0.0083	0.2955 ± 0.0014
D_3 [75]	-	0.5091 ± 0.0064	6.1522 ± 0.1019	0.2798 ± 0.0016	0.5270 ± 0.0022	5.6713 ± 0.0034	0.2687 ± 0.0013
	DDPO [9]	0.5199 ± 0.0046	5.9874 ± 0.0218	0.2831 ± 0.0011	0.5344 ± 0.0036	5.7066 ± 0.0279	0.2708 ± 0.0009
	DPO [12]	0.5158 ± 0.0053	6.2790 ± 0.1282	0.2850 ± 0.0049	0.5369 ± 0.0084	5.7644 ± 0.0046	0.2736 ± 0.0016
	Curriculum-DPO [18]	0.5230 ± 0.0011	6.4337 ± 0.0251	0.3011 ± 0.0034	0.5230 ± 0.0011	6.4337 ± 0.0251	0.3011 ± 0.0034
	Curriculum-DPO++	0.5236 ± 0.0029	6.4572 ± 0.0361	0.3050 ± 0.0005	0.5236 ± 0.0029	6.4572 ± 0.0361	0.3050 ± 0.0005

TABLE 1: Text alignment, aesthetic and human preference scores on datasets D_1 , D_2 and D_3 , obtained by the baseline (pre-trained) LCM and SD models versus the four fine-tuning strategies: DDPO, DPO, Curriculum-DPO and Curriculum-DPO++. The results represent averages over three runs. The best scores on each dataset are highlighted in bold.

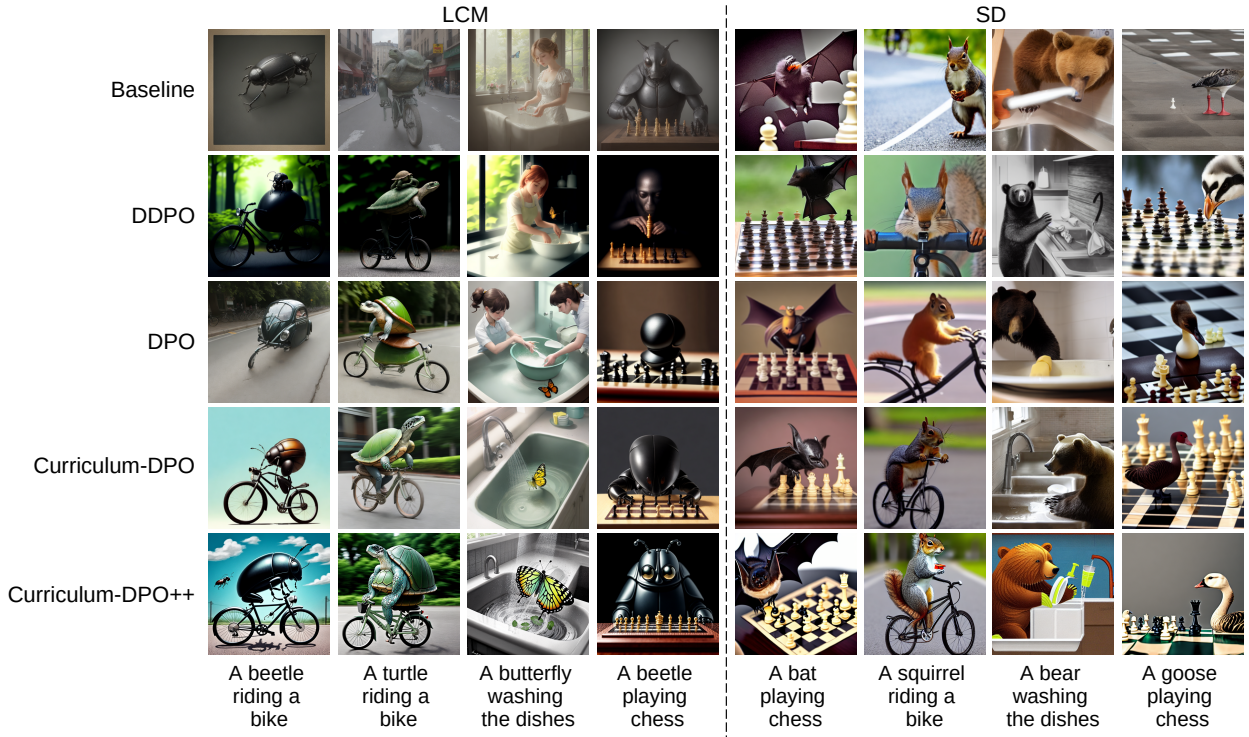


Fig. 2: Qualitative results on dataset D_1 , before and after fine-tuning for the text alignment task. The fine-tuning alternatives are DDPO, DPO, Curriculum-DPO, and Curriculum-DPO++. Best viewed in color.

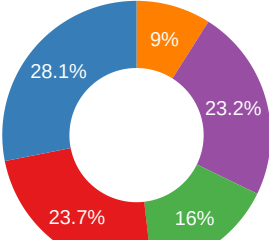
their rank difference. This approach effectively mitigates issues arising from skewed preference score distributions.

Main results. We present quantitative results for Curriculum-DPO and Curriculum-DPO++ versus their competitors in Table 1. Our original Curriculum-DPO [18] surpasses both DDPO and DPO in all scenarios. Moreover, Curriculum-DPO++, the version that integrates our new model-level curriculum, yields a considerable performance boost in most cases, the most significant gains being obtained on human preference for SD on all three datasets. We further complement the quantitative evaluation with qualitative results, depicted in Figure 2. The illustrated images are

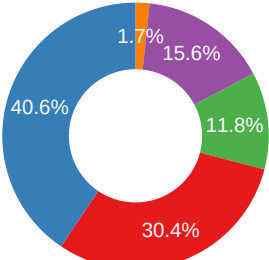
obtained after fine-tuning for text alignment. Although the original Curriculum-DPO does a good job at illustrating animals performing specific activities, our new variant, Curriculum-DPO++, improves the results in several cases. For example, the beetle in the fourth column is generated with a more accurate appearance, and the bear in the seventh column depicts the activity more clearly. Therefore, even in cases where numerical improvements seem limited, such as the text alignment scores for LCM on D_1 (see Table 1), our method demonstrates a distinct perceptual advantage that is clearly visible in the qualitative results. This is further strengthened by the win rates depicted in Figures 3 and 4.

Model	Fine-Tuning Strategy	Dataset D_1 [9]		Dataset D_2 [8]	
		Text Alignment	Human Preference	Text Alignment	Human Preference
LCM	-	0.7243 ± 0.0048	0.2912 ± 0.0021	0.5602 ± 0.0032	0.2610 ± 0.0016
	Curriculum-DPO	0.7224 ± 0.0010	0.2936 ± 0.0003	0.5667 ± 0.0017	0.2775 ± 0.0007
	Curriculum-DPO++	0.7264 ± 0.0029	0.3003 ± 0.0014	0.5577 ± 0.0014	0.2809 ± 0.0010
SD	-	0.6804 ± 0.0052	0.2784 ± 0.0015	0.5997 ± 0.0067	0.2646 ± 0.0011
	Curriculum-DPO	0.7455 ± 0.0022	0.2894 ± 0.0018	0.6242 ± 0.0029	0.2708 ± 0.0018
	Curriculum-DPO++	0.7472 ± 0.0020	0.2947 ± 0.0011	0.6272 ± 0.0032	0.2695 ± 0.0021

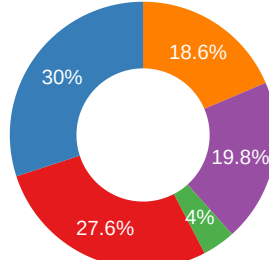
TABLE 2: Text alignment and human preference scores on datasets D_1 and D_2 , obtained by the baseline (pre-trained) LCM and SD models versus the reward-model-free Curriculum-DPO and Curriculum-DPO++. The best scores are highlighted in bold.



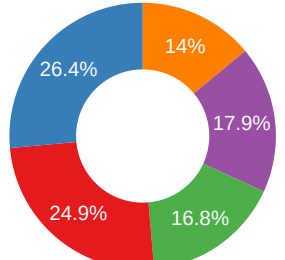
(a) LAION win rates.



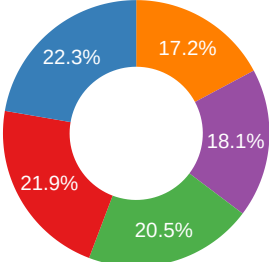
(b) HPSv2 win rates.



(a) LAION win rates.



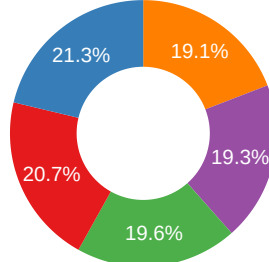
(b) HPSv2 win rates.



(c) LLaVA win rates.

Method

- Curriculum-DPO
- Curriculum-DPO++
- DDPO
- DPO
- SD



(c) LLaVA win rates.

Method

- Curriculum-DPO
- Curriculum-DPO++
- DDPO
- DPO
- LCM

Fig. 3: Preference win rates according to all the three reward models. The comparison is conducted between all the four fine-tuning strategies and the pre-trained SD baseline. For this comparison, we use images generated for the Pick-a-Pic (D_3) test set of prompts. Best viewed in color.

The win rates are computed for each of the three reward models, and are based on how many times each method yields the highest score. More qualitative results are shown in Appendix 6.3.

Reward-model-free results. In Table 2, we present results for Curriculum-DPO and Curriculum-DPO++ using the reward-model-free strategy to create the preference pairs. The proposed reward-model-free strategy based on masking text embeddings demonstrates substantial performance gains compared with the pre-trained LCM and SD baselines across all experimental settings. We observe that the gains are usually higher for SD. Our model-level curriculum learning strategy yields additional enhancements in all scenarios, except for one (SD on dataset D_2). In Figure 6, we showcase some qualitative samples obtained from the fine-tuned SD models on D_1 . These examples demonstrate that our reward-model-free methods, Curriculum-DPO and Curriculum-DPO++, better align with the prompts, while also being more visually appealing. For instance, the rabbit is riding the bike (in line with the prompt) in our images depicted on

Fig. 4: Preference win rates according to all the three reward models. The comparison is conducted between all the four fine-tuning strategies and the pre-trained LCM baseline. For this comparison, we use images generated for the Pick-a-Pic (D_3) test set of prompts. Best viewed in color.

the first column, but the rabbit just stays on the fence in the baseline image.

Ablations. The original Curriculum-DPO has several hyperparameters. We showcase the impact of each hyperparameter through a series of ablation studies. First, we explore different values of β , when fine-tuning LCM via Consistency-DPO. Results with $\beta \in \{50, \dots, 500\}$ are shown in Figure 5a. When $\beta \geq 200$, the fine-tuning outperforms the baseline. In Figure 5b, we search for the optimal value for the number of training iterations per curriculum batch, K , in terms of HPSv2 scores. For all of the explored values between 100 and 500, we obtain better results than the baseline. Further, in Figure 5c, we explore how many curriculum batches are needed, considering values between 3 and 7. Curriculum-DPO consistently surpasses the baseline, regardless of the number of training batches. Finally, in Figure 5d, we assess the impact of the number of training images generated per prompt, from $M = 5$ to $M = 500$. For reference, we include the results of DPO and DDPO based on $M = 500$ images per prompt. Notably, Curriculum-DPO is able to

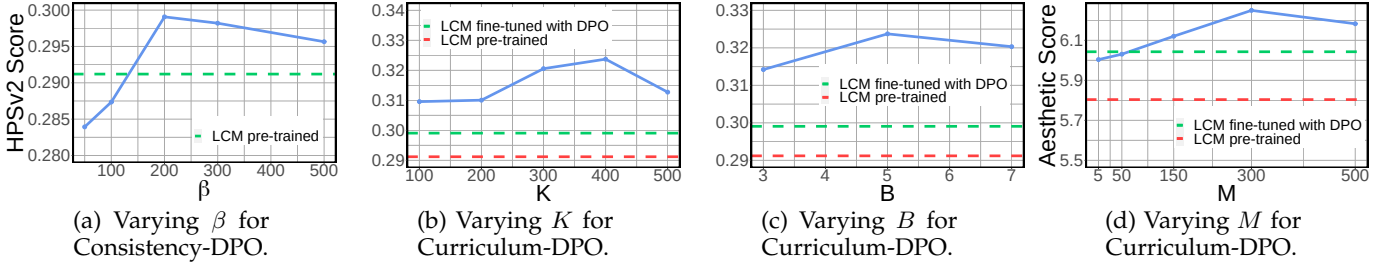


Fig. 5: Ablation results obtained by (a) varying the hyperparameter β for Consistency-DPO (in blue), (b) the number of training iterations per batch K for Curriculum-DPO (in blue), (c) the number of batches B for Curriculum-DPO (in blue), and (d) the number of training images per prompt M (in blue). Fine-tuned LCM models are compared with the pre-trained LCM baseline on the human preference and visual appeal tasks, where scores are given by the HPSv2 reward model and LAION Aesthetics Predictor, respectively. Best viewed in color.

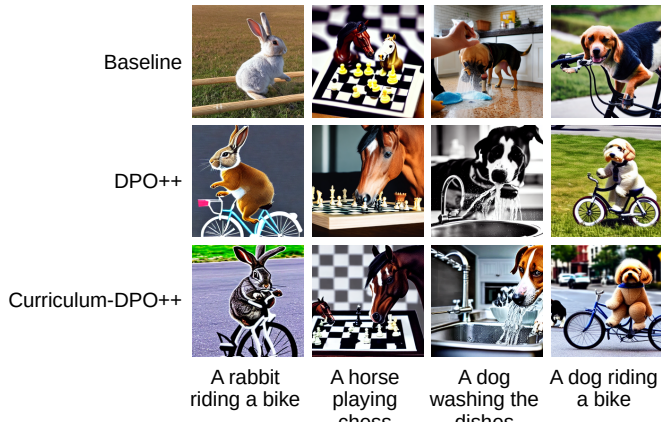


Fig. 6: Qualitative results on dataset D_1 , before and after fine-tuning for the text alignment task with our reward-model-free methodology. Best viewed in color.

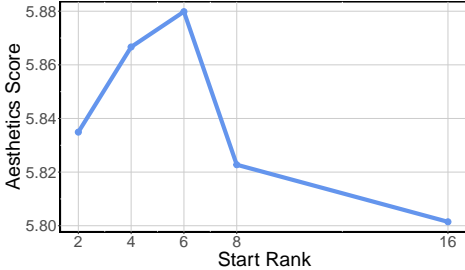


Fig. 7: Ablation study on the start rank r_{start} for the LoRA matrices. The study is conducted for SD on D_2 using the LAION Aesthetics reward. For this ablation, the final rank r_{end} is fixed to 16.

obtain comparable performance with DPO and DDPO, while using $10 \times$ less training images. Moreover, Curriculum-DPO outperforms the baseline LCM regardless of the number of training images. In general, we observe that Curriculum-DPO maintains its superiority over DPO under various hyperparameter configurations.

We next present additional ablations for the contributions included in Curriculum-DPO++. To determine the optimal value for the start dimension r_{start} of the LoRA matrices, we conduct an ablation study using SD on dataset D_2 , using the LAION Aesthetics reward. To ensure a fair comparison with the original Curriculum-DPO, we do not vary r_{end} . Instead, we fixed this parameter to match the baseline configuration exactly. We present the corresponding results in Figure 7.

	Progressive Rank	Progressive Layers	Aesthetics
	✗	✗	5.7060
	✓	✗	5.7400
	✗	✓	5.8015
	✓	✓	5.8798

TABLE 3: Ablation study on the key components of the model-level curriculum added on top of Curriculum-DPO. The study is conducted on D_2 with the SD fine-tuned via the LAION Aesthetics reward model.

Curriculum-DPO reaches an aesthetics score of 5.706 (see Table 1), while Curriculum-DPO++ is consistently above 5.8 (see Figure 7), indicating that model-level curriculum is useful, no matter how r_{start} is set.

The model-level curriculum progressively increases both the rank of the LoRA matrices and the number of layers that are being updated via LoRA. In Table 3, we showcase the impact of each component of the model-level curriculum, both in isolation as well as in the combined configuration. Two primary conclusions can be drawn from these results. First, we observe that every variation of our method consistently surpasses the baseline, confirming the robustness of our model-level curriculum across all tested scenarios. Second, the results indicate that the two components are effectively orthogonal. Consequently, when combined, they produce a substantial performance boost that exceeds the gains of either component individually.

5 CONCLUSION

Building on top of our previous work introducing data-level curriculum into DPO, we proposed an enhanced framework, deemed Curriculum-DPO++, that gracefully integrates data-level and model-level curricula. Curriculum-DPO++ increases learning capacity at the same pace with data complexity, enabling better generalization. Through comprehensive experiments on three datasets and three downstream tasks, we demonstrated consistent performance gains due to our model-level progressive training. Moreover, our second contribution, a reward-model-free extension of Curriculum-DPO++, which is based on text embedding masking, proved to be a viable fine-tuning solution, showing improvements in almost all text alignment and human preference scenarios. In general, Curriculum-DPO++ demonstrated both quantitative and qualitative enhancements, producing models that are more inclined to follow the input prompt and generate images that are more visually appealing. We conducted

ablation experiments to attest that each contribution is empirically relevant and to determine the robustness to hyperparameter variations. Our ablation studies showed that Curriculum-DPO and Curriculum-DPO++ are robust to suboptimal hyperparameter settings, obtaining consistent performance gains over the corresponding baselines for a broad range of hyperparameter configurations.

In future work, we intend to apply Curriculum-DPO++ beyond image generation, e.g. to fine-tune Large Language Models. In natural language processing, curricula could explicitly be defined for textual data, taking into account prompt complexity or reasoning depth.

ACKNOWLEDGMENTS

This work was supported by a grant of the Ministry of Research, Innovation and Digitization, CNCS - UEFISCDI, project number PN-IV-P1-PCE-2023-0354, within PNCDI IV.

REFERENCES

- [1] F.-A. Croitoru, V. Hondru, R. T. Ionescu, and M. Shah, "Diffusion models in vision: A survey," *IEEE Transactions on Pattern Analysis and Machine Intelligence*, vol. 45, pp. 10850–10869, 2023.
- [2] J. Ho, A. Jain, and P. Abbeel, "Denoising diffusion probabilistic models," in *Proceedings of NeurIPS*, vol. 33, pp. 6840–6851, 2020.
- [3] J. Sohl-Dickstein, E. Weiss, N. Maheswaranathan, and S. Ganguli, "Deep unsupervised learning using non-equilibrium thermodynamics," in *Proceedings of ICML*, pp. 2256–2265, 2015.
- [4] Y. Song and S. Ermon, "Generative modeling by estimating gradients of the data distribution," in *Proceedings of NeurIPS*, vol. 32, pp. 11918–11930, 2019.
- [5] O. Avrahami, D. Lischinski, and O. Fried, "Blended diffusion for text-driven editing of natural images," in *Proceedings of CVPR*, pp. 18208–18218, 2022.
- [6] S. Gu, D. Chen, J. Bao, F. Wen, B. Zhang, D. Chen, L. Yuan, and B. Guo, "Vector quantized diffusion model for text-to-image synthesis," in *Proceedings of CVPR*, pp. 10696–10706, 2022.
- [7] R. Rombach, A. Blattmann, D. Lorenz, P. Esser, and B. Ommer, "High-Resolution Image Synthesis with Latent Diffusion Models," in *Proceedings of CVPR*, pp. 10684–10695, 2022.
- [8] C. Saharia, W. Chan, S. Saxena, L. Li, J. Whang, E. L. Denton, K. Ghasemipour, R. Gontijo Lopes, B. Karagol Ayan, T. Salimans, et al., "Photorealistic text-to-image diffusion models with deep language understanding," in *Proceedings of NeurIPS*, pp. 36479–36494, 2022.
- [9] K. Black, M. Janner, Y. Du, I. Kostrikov, and S. Levine, "Training Diffusion Models with Reinforcement Learning," in *Proceedings of ICLR*, 2024.
- [10] Y. Fan, O. Watkins, Y. Du, H. Liu, M. Ryu, C. Boutilier, P. Abbeel, M. Ghavamzadeh, K. Lee, and K. Lee, "DPOK: Reinforcement Learning for Fine-tuning Text-to-Image Diffusion Models," in *Proceedings of NeurIPS*, vol. 36, pp. 79858–79885, 2023.
- [11] S. Luo, Y. Tan, S. Patil, D. Gu, P. von Platen, A. Passos, L. Huang, J. Li, and H. Zhao, "LCM-LoRA: A Universal Stable-Diffusion Acceleration Module," *arXiv preprint arXiv:2311.05556*, 2023.
- [12] B. Wallace, M. Dang, R. Rafailov, L. Zhou, A. Lou, S. Purushwalkam, S. Ermon, C. Xiong, S. Joty, and N. Naik, "Diffusion Model Alignment Using Direct Preference Optimization," in *Proceedings of CVPR*, pp. 8228–8238, 2024.
- [13] P. F. Christiano, J. Leike, T. Brown, M. Martic, S. Legg, and D. Amodei, "Deep Reinforcement Learning from Human Preferences," in *Proceedings of NeurIPS*, vol. 30, pp. 4302–4310, 2017.
- [14] E. J. Hu, P. Wallis, Z. Allen-Zhu, Y. Li, S. Wang, L. Wang, W. Chen, et al., "LoRA: Low-Rank Adaptation of Large Language Models," in *Proceedings of ICLR*, 2022.
- [15] R. Rafailov, A. Sharma, E. Mitchell, C. D. Manning, S. Ermon, and C. Finn, "Direct Preference Optimization: Your Language Model is Secretly a Reward Model," in *Proceedings of NeurIPS*, vol. 36, pp. 53728–53741, 2023.
- [16] R. Schwartz, J. Dodge, N. A. Smith, and O. Etzioni, "Green AI," *Communications of the ACM*, vol. 63, no. 12, pp. 54–63, 2020.
- [17] E. Strubell, A. Ganesh, and A. Mccallum, "Energy and Policy Considerations for Deep Learning in NLP," in *Proceedings of ACL*, pp. 3645–3650, 2019.
- [18] F.-A. Croitoru, V. Hondru, R. T. Ionescu, N. Sebe, and M. Shah, "Curriculum direct preference optimization for diffusion and consistency models," in *Proceedings of CVPR*, pp. 2824–2834, 2025.
- [19] Y. Bengio, J. Louradour, R. Collobert, and J. Weston, "Curriculum Learning," in *Proceedings of ICML*, pp. 41–48, 2009.
- [20] N. Reimers and I. Gurevych, "Sentence-BERT: Sentence Embeddings using Siamese BERT-Networks," in *Proceedings of EMNLP*, pp. 3982–3992, 2019.
- [21] H. Liu, C. Li, Q. Wu, and Y. J. Lee, "Visual instruction tuning," in *Proceedings of NeurIPS*, vol. 36, pp. 34892–34916, 2023.
- [22] C. Schuhmann, "LAION-Aesthetics." <https://laion.ai/blog/laion-aesthetics/>, 2022.
- [23] X. Wu, Y. Hao, K. Sun, Y. Chen, F. Zhu, R. Zhao, and H. Li, "Human Preference Score v2: A Solid Benchmark for Evaluating Human Preferences of Text-to-Image Synthesis," *arXiv preprint arXiv:2306.09341*, 2023.
- [24] Y. Song, J. Sohl-Dickstein, D. P. Kingma, A. Kumar, S. Ermon, and B. Poole, "Score-Based Generative Modeling through Stochastic Differential Equations," in *Proceedings of ICLR*, 2021.
- [25] P. Dhariwal and A. Nichol, "Diffusion models beat GANs on image synthesis," in *Proceedings of NeurIPS*, vol. 34, pp. 8780–8794, 2021.
- [26] A. Ramesh, P. Dhariwal, A. Nichol, C. Chu, and M. Chen, "Hierarchical text-conditional image generation with CLIP latents," *arXiv preprint arXiv:2204.06125*, 2022.
- [27] R. Rombach, A. Blattmann, and B. Ommer, "Text-Guided Synthesis of Artistic Images with Retrieval-Augmented Diffusion Models," *arXiv preprint arXiv:2207.13038*, 2022.
- [28] D. Baranchuk, I. Rubachev, A. Voynov, V. Khrulkov, and A. Babenko, "Label-Efficient Semantic Segmentation with Diffusion Models," in *Proceedings of ICLR*, 2022.
- [29] C. Meng, Y. Song, J. Song, J. Wu, J.-Y. Zhu, and S. Ermon, "SDEdit: Guided Image Synthesis and Editing with Stochastic Differential Equations," in *Proceedings of ICLR*, 2021.
- [30] C. Saharia, W. Chan, H. Chang, C. Lee, J. Ho, T. Salimans, D. Fleet, and M. Norouzi, "Palette: Image-to-image diffusion models," in *Proceedings of SIGGRAPH*, pp. 1–10, 2022.
- [31] C.-H. Chao, W.-F. Sun, B.-W. Cheng, Y.-C. Lo, C.-C. Chang, Y.-L. Liu, Y.-L. Chang, C.-P. Chen, and C.-Y. Lee, "Denoising Likelihood Score Matching for Conditional Score-Based Data Generation," in *Proceedings of ICLR*, 2022.
- [32] J. Ho, C. Saharia, W. Chan, D. J. Fleet, M. Norouzi, and T. Salimans, "Cascaded Diffusion Models for High Fidelity Image Generation," *Journal of Machine Learning Research*, vol. 23, no. 47, pp. 1–33, 2022.
- [33] T. Salimans and J. Ho, "Progressive distillation for fast sampling of diffusion models," in *Proceedings of ICLR*, 2022.
- [34] A. Lugmayr, M. Danelljan, A. Romero, F. Yu, R. Timofte, and L. Van Gool, "RePaint: Inpainting using Denoising Diffusion Probabilistic Models," in *Proceedings of CVPR*, pp. 11461–11471, 2022.
- [35] A. Q. Nichol, P. Dhariwal, A. Ramesh, P. Shyam, P. Mishkin, B. McGrew, I. Sutskever, and M. Chen, "GLIDE: Towards Photorealistic Image Generation and Editing with Text-Guided Diffusion Models," in *Proceedings of ICML*, pp. 16784–16804, 2022.
- [36] M. Daniels, T. Maunu, and P. Hand, "Score-based generative neural networks for large-scale optimal transport," in *Proceedings of NeurIPS*, pp. 12955–12965, 2021.
- [37] C. Saharia, J. Ho, W. Chan, T. Salimans, D. J. Fleet, and M. Norouzi, "Image super-resolution via iterative refinement," *IEEE Transactions on Pattern Analysis and Machine Intelligence*, vol. 45, no. 4, pp. 4713–4726, 2022.
- [38] H. Chung and J. C. Ye, "Score-based diffusion models for accelerated MRI," *Medical Image Analysis*, vol. 80, p. 102479, 2022.
- [39] J. Wyatt, A. Leach, S. M. Schmon, and C. G. Willcocks, "AnoDDPM: Anomaly Detection with Denoising Diffusion Probabilistic Models using Simplex Noise," in *Proceedings of CVPR*, pp. 650–656, 2022.
- [40] L. Liu, Y. Ren, Z. Lin, and Z. Zhao, "Pseudo Numerical Methods for Diffusion Models on Manifolds," in *Proceedings of ICLR*, 2022.
- [41] A. Q. Nichol and P. Dhariwal, "Improved denoising diffusion probabilistic models," in *Proceedings of ICML*, pp. 8162–8171, 2021.
- [42] J. Song, C. Meng, and S. Ermon, "Denoising Diffusion Implicit Models," in *Proceedings of ICLR*, 2021.
- [43] Y. Song, P. Dhariwal, M. Chen, and I. Sutskever, "Consistency models," in *Proceedings of ICML*, pp. 32211–32252, 2023.

[44] S. Luo, Y. Tan, L. Huang, J. Li, and H. Zhao, "Latent consistency models: Synthesizing high-resolution images with few-step inference," *arXiv preprint arXiv:2310.04378*, 2023.

[45] Y. Song and P. Dhariwal, "Improved Techniques for Training Consistency Models," in *Proceedings of ICLR*, 2024.

[46] J. Ho and T. Salimans, "Classifier-Free Diffusion Guidance," in *Proceedings of NeurIPS Workshop on DGMs and Applications*, 2021.

[47] L. Zhang, A. Rao, and M. Agrawala, "Adding Conditional Control to Text-to-Image Diffusion Models," in *Proceedings of ICCV*, pp. 3836–3847, 2023.

[48] K. Papineni, S. Roukos, T. Ward, and W.-J. Zhu, "BLEU: A Method for Automatic Evaluation of Machine Translation," in *Proceedings of ACL*, pp. 311–318, 2002.

[49] Y. Bai, S. Kadavath, S. Kundu, A. Askell, J. Kernion, A. Jones, A. Chen, A. Goldie, A. Mirhoseini, C. McKinnon, et al., "Constitutional AI: Harmlessness from AI feedback," *arXiv preprint arXiv:2212.08073*, 2022.

[50] A. Havrilla, Y. Du, S. C. Raparthy, C. Nalmpantis, J. Dwivedi-Yu, M. Zhuravinsky, E. Hambro, S. Sukhbaatar, and R. Raileanu, "Teaching large language models to reason with reinforcement learning," in *Proceedings of AI4Math*, 2024.

[51] D. M. Ziegler, N. Stiennon, J. Wu, T. B. Brown, A. Radford, D. Amodei, P. Christiano, and G. Irving, "Fine-Tuning Language Models from Human Preferences," *arXiv preprint arXiv:1909.08593*, 2020.

[52] K. Lee, H. Liu, M. Ryu, O. Watkins, Y. Du, C. Boutilier, P. Abbeel, M. Ghavamzadeh, and S. S. Gu, "Aligning text-to-image models using human feedback," *arXiv preprint arXiv:2302.12192*, 2023.

[53] L. Ouyang, J. Wu, X. Jiang, D. Almeida, C. Wainwright, P. Mishkin, C. Zhang, S. Agarwal, K. Slama, A. Ray, et al., "Training language models to follow instructions with human feedback," in *Proceedings of NeurIPS*, vol. 35, pp. 27730–27744, 2022.

[54] J. Schulman, F. Wolski, P. Dhariwal, A. Radford, and O. Klimov, "Proximal policy optimization algorithms," *arXiv preprint arXiv:1707.06347*, 2017.

[55] P. Soviany, R. T. Ionescu, P. Rota, and N. Sebe, "Curriculum learning: A survey," *International Journal of Computer Vision*, vol. 130, no. 6, pp. 1526–1565, 2022.

[56] Y. Wang, Y. Yue, R. Lu, T. Liu, Z. Zhong, S. Song, and G. Huang, "EfficientTrain: Exploring Generalized Curriculum Learning for Training Visual Backbones," in *Proceedings of ICCV*, pp. 5852–5864, 2023.

[57] X. Wang, Y. Zhou, H. Chen, and W. Zhu, "Curriculum Learning for Multimedia in the Era of Large Language Models," in *Proceedings of ACMMM*, pp. 11296–11297, 2024.

[58] R. T. Ionescu, B. Alexe, M. Leordeanu, M. Popescu, D. P. Papadopoulos, and V. Ferrari, "How hard can it be? estimating the difficulty of visual search in an image," in *Proceedings of CVPR*, pp. 2157–2166, 2016.

[59] L. Jiang, D. Meng, Q. Zhao, S. Shan, and A. Hauptmann, "Self-paced curriculum learning," in *Proceedings of AAAI*, vol. 29, pp. 2694–2700, 2015.

[60] M. Kumar, B. Packer, and D. Koller, "Self-paced learning for latent variable models," in *Proceedings of NeurIPS*, vol. 23, pp. 1189–1197, 2010.

[61] M. Lao, Y. Guo, Y. Liu, W. Chen, N. Pu, and M. S. Lew, "From superficial to deep: Language bias driven curriculum learning for visual question answering," in *Proceedings of ACMMM*, pp. 3370–3379, 2021.

[62] P. Soviany, R. T. Ionescu, P. Rota, and N. Sebe, "Curriculum self-paced learning for cross-domain object detection," *Computer Vision and Image Understanding*, vol. 204, pp. 103–166, 2021.

[63] C. Yu, J. Zhao, Y. Liu, S. Zhao, Y. Dai, and X. Yue, "From Easy to Hard: Progressive Active Learning Framework for Infrared Small Target Detection with Single Point Supervision," in *Proceedings of ICCV*, pp. 2588–2598, 2025.

[64] T. Karras, T. Aila, S. Laine, and J. Lehtinen, "Progressive growing of GANs for improved quality, stability, and variation," in *Proceedings of ICLR*, 2018.

[65] N. Madan, N.-C. Ristea, K. Nasrollahi, T. B. Moeslund, and R. T. Ionescu, "CL-MAE: Curriculum-Learned Masked Autoencoders," in *Proceedings of WACV*, pp. 2492–2502, 2024.

[66] P. Morerio, J. Cavazza, R. Volpi, R. Vidal, and V. Murino, "Curriculum dropout," in *Proceedings of ICCV*, pp. 3544–3552, 2017.

[67] S. Sinha, A. Garg, and H. Larochelle, "Curriculum by Smoothing," in *Proceedings of NeurIPS*, pp. 21653–21664, 2020.

[68] F.-A. Croitoru, N.-C. Ristea, R. T. Ionescu, and N. Sebe, "Learning rate curriculum," *International Journal of Computer Vision*, vol. 133, no. 1, pp. 291–314, 2025.

[69] T. Doan, J. Monteiro, I. Albuquerque, B. Mazoure, A. Durand, J. Pineau, and R. D. Hjelm, "On-line adaptative curriculum learning for GANs," in *Proceedings of AAAI*, vol. 33, pp. 3470–3477, 2019.

[70] K. Ghasedi, X. Wang, C. Deng, and H. Huang, "Balanced self-paced learning for generative adversarial clustering network," in *Proceedings of CVPR*, pp. 4391–4400, 2019.

[71] P. Soviany, C. Ardei, R. T. Ionescu, and M. Leordeanu, "Image difficulty curriculum for generative adversarial networks (CuGAN)," in *Proceedings of WACV*, pp. 3463–3472, 2020.

[72] J.-Y. Kim, H. Go, S. Kwon, and H.-G. Kim, "Denoising task difficulty-based curriculum for training diffusion models," in *Proceedings of ICLR*, 2025.

[73] T. Xu, P. Mi, R. Wang, and Y. Chen, "Towards Faster Training of Diffusion Models: An Inspiration of A Consistency Phenomenon," *arXiv preprint arXiv:2404.07946*, 2024.

[74] S. Na, Y. Kim, and H. Lee, "Boost Your Human Image Generation Model via Direct Preference Optimization," in *Proceedings of CVPR*, pp. 23551–23562, 2025.

[75] Y. Kirstain, A. Polyak, U. Singer, S. Matiana, J. Penna, and O. Levy, "Pick-a-pic: An open dataset of user preferences for text-to-image generation," in *Proceedings of NeurIPS*, 2023.

[76] A. Radford, J. W. Kim, C. Hallacy, A. Ramesh, G. Goh, S. Agarwal, G. Sastry, A. Askell, P. Mishkin, J. Clark, G. Krueger, and I. Sutskever, "Learning transferable visual models from natural language supervision," in *Proceedings of ICML*, vol. 139, pp. 8748–8763, 2021.

[77] T. Karras, S. Laine, M. Aittala, J. Hellsten, J. Lehtinen, and T. Aila, "Analyzing and improving the image quality of StyleGAN," in *Proceedings of CVPR*, pp. 8110–8119, 2020.

[78] D. Kingma, T. Salimans, B. Poole, and J. Ho, "Variational diffusion models," in *Proceedings of NeurIPS*, vol. 34, pp. 21696–21707, 2021.

[79] A. Vahdat, K. Kreis, and J. Kautz, "Score-based generative modeling in latent space," in *Proceedings of NeurIPS*, vol. 34, pp. 11287–11302, 2021.

[80] B. D. Anderson, "Reverse-time diffusion equation models," *Stochastic Processes and their Applications*, vol. 12, no. 3, pp. 313–326, 1982.

[81] X. B. Peng, A. Kumar, G. Zhang, and S. Levine, "Advantage-Weighted Regression: Simple and Scalable Off-Policy Reinforcement Learning," *arXiv preprint arXiv:1910.00177*, 2019.

[82] J. Peters and S. Schaal, "Reinforcement learning by reward-weighted regression for operational space control," in *Proceedings of ICML*, p. 745–750, 2007.

6 APPENDIX

6.1 Detailed Preliminaries

Diffusion models. Diffusion models [1]–[4], [7], [24], [77]–[79] are a class of generative models trained to reverse a process that progressively inserts Gaussian noise across T steps into the original data samples, transforming them into standard Gaussian noise. Formally, the forward process defined by:

$$x_t = \alpha_t x_0 + \sigma_t \epsilon, \epsilon \sim \mathcal{N}(0, \mathbf{I}) \quad (9)$$

transforms the original samples $x_0 \sim p(x_0)$ into noisy versions x_t , following the noise schedule implied by the time-dependent predefined functions $(\alpha_t)_{t=1}^T$ and $(\sigma_t)_{t=1}^T$. The model is trained to estimate the noise ϵ added in the forward step defined in Eq. (9), by minimizing the following objective:

$$\mathcal{L}_{\text{simple}} = \mathbb{E}_{t \sim \mathcal{U}(1, T), \epsilon \sim \mathcal{N}(0, \mathbf{I}), x_0 \sim p(x_0)} \|\epsilon_t - \epsilon_\theta(x_t, t)\|^2. \quad (10)$$

The generation process involves denoising, starting from a sample of standard Gaussian noise, denoted as $x_T \sim \mathcal{N}(0, \mathbf{I})$. It then follows the transitions outlined in Eq. (11) to produce novel samples:

$$p_\theta(x_{t-1}|x_t) = \mathcal{N}\left(x_{t-1}; \mu_\theta(x_t, t), \sigma_{t|t-1}^2 \frac{\sigma_{t-1}^2}{\sigma_t^2}\right), \quad (11)$$

with $\mu_\theta(x_t, t) = \frac{1}{\alpha_{t|t-1}} \left(x_t - \frac{\epsilon_\theta(x_t, t) \sigma_{t|t-1}^2}{\sigma_t} \right)$, where $\sigma_{t|t-1}^2 = \sigma_t^2 - \alpha_{t|t-1}^2 \sigma_{t-1}^2$ and $\alpha_{t|t-1} = \frac{\alpha_t}{\alpha_{t-1}}$.

The forward process can also be defined in a continuous time manner [24], as a stochastic differential equation (SDE):

$$dx_t = f(t)x_t dt + g(t)d\omega_t, t \in [0, T], \quad (12)$$

where, given the notations from Eq. (9), we can write $f(t) = \frac{d \log \alpha(t)}{dt}$ and $g^2(t) = \frac{d \sigma^2(t)}{dt} - 2 \frac{d \log \alpha(t)}{dt} \cdot \sigma^2(t)$, and ω_t is the standard Brownian motion.

Furthermore, the diffusion process described by the SDE from Eq. (12) can be reversed by another diffusion process given by a reverse-time SDE [24], [80]. In addition, Song *et al.* [24] showed that the reverse SDE has a corresponding ordinary differential equation (ODE), called Probability flow-ODE (PF-ODE), with the following form:

$$dx_t = f(t)x_t dt + \frac{g^2(t)}{2\sigma(t)} \epsilon_\theta(x_t, t). \quad (13)$$

Consistency models. Consistency models [43]–[45] are a new class of generative models. These models operate on the idea of training a model to associate each point along a trajectory of the PF-ODE (Eq. (13)) to the initial point of the respective trajectory, which corresponds to the denoised sample. Such models can either be trained from scratch or through distillation from a pre-trained diffusion model. In our study, we employ the distillation method, so we next detail this approach.

Given a solution trajectory $\{x_t\}_{t \in [\delta, T]}$ of the PF-ODE defined in Eq. (13), where $\delta \rightarrow 0$, the training of a consistency model $f_\phi(x_t, t)$ involves enforcing the self-consistency property across this trajectory, such that, $\forall t, t' \in [\delta, T]$, the condition $f_\phi(x_t, t) = f_\phi(x_{t'}, t')$ holds. The loss function designed to achieve this self-consistency is described as follows:

$$\mathcal{L}_{\text{CD}}(\phi) = d(f_\phi(x_{t_{n+1}}, t_{n+1}), f_{\phi^-}(\hat{x}_{t_n}^\theta, t_n)), \quad (14)$$

where d is a distance metric, $n \sim \mathcal{U}(1, N)$, N is the discretization length of the interval $[0, T]$, ϕ are the trainable parameters of the consistency model and ϕ^- is a running average of ϕ . The term $\hat{x}_{t_n}^\theta$ represents a one-step denoised version of $x_{t_{n+1}}$, obtained by applying an ODE solver on the PF-ODE. The solver operates using a pre-trained diffusion model, $\epsilon_\theta(x_{t_n}, t_n)$.

Direct Preference Optimization (DPO). Training pipelines based on Reinforcement Learning with Human Feedback (RLHF) [51] have been highly successful in aligning Large Language Models to human preferences. These pipelines feature an initial phase where a reward model is trained using examples ranked by humans, followed by a reinforcement learning phase where the policy model is fine-tuned to align with the learned reward model. In this context, Rafailov *et al.* [15] introduced DPO as an alternative to the previous pipeline, which bypasses the training of the reward model and directly optimizes the policy model using the ranked examples.

The training dataset contains triplets of the form (c, x_0^w, x_0^l) , where x_0^w denotes the favored (winning) sample, x_0^l the unfavored (losing) one, and c is a condition used to generate both samples. RLHF trains a reward model by maximizing the likelihood $p(x_0^w \prec x_0^l | c)$ ¹, which, under the Bradley-Terry (BT) model, has the following form:

$$p_{\text{BT}}(x_0^w \prec x_0^l | c) = \sigma(r_\varphi(x_0^w, c) - r_\varphi(x_0^l, c)), \quad (15)$$

where σ denotes the sigmoid function and r_φ is the reward model parameterized by the trainable parameters φ . The training objective for the reward model is the negative log-likelihood:

$$\mathcal{L}_{\text{BT}} = -\mathbb{E}_{x_0^w, x_0^l, c} [\log \sigma(r_\varphi(x_0^w, c) - r_\varphi(x_0^l, c))]. \quad (16)$$

After training the reward model $r_\varphi(x_0, c)$, RLHF optimizes a conditional generative model $p_\theta(x_0 | c)$ to maximize the reward $r_\varphi(x_0, c)$ and, at the same time, controls the deviance from a reference model $p_{\text{ref}}(x_0, c)$ through a Kullback–Leibler (KL) divergence term:

$$\max_{\theta} \mathbb{E}_{c, x_0 \sim p_\theta(x_0 | c)} [r_\varphi(x_0, c) - \beta \cdot \text{KL}(p_\theta(x_0 | c), p_{\text{ref}}(x_0 | c))], \quad (17)$$

where β controls the importance of the divergence term.

To derive the DPO objective, Rafailov *et al.* [15] write the optimal policy model p_θ^* of Eq. (17) as a function of the reward and the reference model, as shown in prior works [81], [82]:

$$p_\theta^*(x_0 | c) = \frac{p_{\text{ref}}(x_0 | c) \cdot \exp\left(\frac{r(x_0, c)}{\beta}\right)}{Z(c)}, \quad (18)$$

where $Z(c) = \sum_{x_0} p_{\text{ref}}(x_0 | c) \cdot \exp\left(\frac{r(x_0, c)}{\beta}\right)$ is a normalization constant. Further, from Eq. (18), Rafailov *et al.* [15] rewrite the reward as:

$$r(x_0, c) = \beta \left(\log \frac{p_\theta^*(x_0 | c)}{p_{\text{ref}}(x_0 | c)} + \log Z(c) \right). \quad (19)$$

Finally, the DPO objective is obtained after replacing the

¹ $a \prec b$ denotes that a precedes b in the ranking implied by the reward model.

Algorithm 2: Curriculum-DPO++ (for diffusion models)

Input: $\{(x_{0,i}, c)\}_{i=1}^M$ - the training samples, $r_\varphi(x_0, c)$ - the reward model which can be conditioned on c , B - the number of batches for splitting the set of pairs, α_t, σ_t - the parameters of the noise schedule, T - the last diffusion time step, β - DPO hyperparameter to control the divergence from the initial pre-trained state, σ - the sigmoid function, η - the learning rate, $\{H_k\}_{k=1}^B$ - the number of training iterations after including the k -th batch, $\{G_k\}_{k=1}^B$ - the trainable layers after including the k -th batch, ϕ - the pre-trained weights of the reference model, $\mathbf{r}_{\text{start}}$ - the rank of the LoRA adaptation matrices at the start of the training, \mathbf{r}_{end} - the rank of the LoRA adaptation matrices at the end of the training, δ - the rank update rate.

Output: θ - the trained weights of the generative model.

1 $\hat{X} \leftarrow \{(x_{0,i}, c) | r_\varphi(x_{0,i}, c) \leq r_\varphi(x_{0,i-1}, c), i = \{2, 3, \dots, M\}\}$; \triangleleft sort the samples in descending order of the rewards

2 $S \leftarrow \{(x_{0,i}, x_{0,j}, c) | i, j \in \{1, \dots, M\}; i < j; x_{0,i}, x_{0,j} \in \hat{X}, r_\varphi(x_{0,i}, c) > r_\varphi(x_{0,j}, c)\}$; \triangleleft create pairs of examples using the order from \hat{X}

3 $L_k \leftarrow \left\{ \frac{(M-1) \cdot (B-k)}{B} \right\}_{k=1}^B$; \triangleleft the minimum preference limits of the batches

4 $R_k \leftarrow \left\{ \frac{(M-1) \cdot (B-(k-1))}{B} \right\}_{k=1}^B$; \triangleleft the maximum preference limits of the batches

5 $S_k \leftarrow \{(x_0^w, x_0^l, c) | (x_0^w, x_0^l) = (x_{0,i}, x_{0,j}); L_k < j - i \leq R_k; (x_{0,i}, x_{0,j}, c) \in S\}_{k=1}^B$; \triangleleft the batches of increasingly difficult pairs

6 $\mathbf{r} \leftarrow \{\mathbf{r}_k | k \in \{1, \dots, B\}, \mathbf{r}_1 = \mathbf{r}_{\text{start}}, \mathbf{r}_{k+1} = \min(\mathbf{r}_{\text{end}}, \mathbf{r}_k \cdot \delta)\}$; \triangleleft the ranks of the low-rank matrices in LoRA

7 $\text{LoRA}_k = \{(A_i^{\mathbf{r}_k}, C_i^{\mathbf{r}_k}) | i \in G_k, A_i^{\mathbf{r}_k} \sim \mathcal{N}(0, \sigma), C_i^{\mathbf{r}_k} = \mathbf{0}_{m \times \mathbf{r}_k}\}_{k=1}^B$; \triangleleft initialization of LoRA matrices

8 $P \leftarrow \emptyset$; \triangleleft current training set

9 $G \leftarrow \emptyset$; \triangleleft current trainable layers

10 **foreach** $k \in \{1, \dots, B\}$ **do**

11 $P \leftarrow P \cup S_k$; \triangleleft include a new batch in the training

12 $G^{\text{new}} \leftarrow \text{LoRA}_k$; \triangleleft include new set of trainable layers

13 **foreach** $(A_i^{\mathbf{r}_k}, C_i^{\mathbf{r}_k}) \in G^{\text{new}}$ **do**

14 **if** $i < |G|$ **then**

15 // transfer the previously learned weights to the new matrices

16 $A_i^{\mathbf{r}_{k-1}}, C_i^{\mathbf{r}_{k-1}} \leftarrow G_i$;

17 $A_i^{\mathbf{r}_k}[:, \mathbf{r}_{k-1}, :] \leftarrow A_i^{\mathbf{r}_{k-1}}$;

18 $C_i^{\mathbf{r}_k}[:, :, \mathbf{r}_{k-1}] \leftarrow C_i^{\mathbf{r}_{k-1}}$;

19 $G \leftarrow G^{\text{new}}$;

20 **foreach** $i \in \{1, \dots, H_k\}$ **do**

21 $(x_0^w, x_0^l, c) \sim \mathcal{U}(P); t \sim \mathcal{U}\{1, \dots, T\}; \epsilon^w, \epsilon^l \sim \mathcal{N}(0, \mathbf{I})$;

22 $x_t^w \leftarrow \alpha_t x_0^w + \sigma_t \epsilon^w$; \triangleleft forward process

23 $x_t^l \leftarrow \alpha_t x_0^l + \sigma_t \epsilon^l$; \triangleleft forward process

24 $\mathcal{L}_{\text{Diff-DPO}}(\theta, G) \leftarrow -\left[\log \sigma\left(-\beta T \left(\left(\|\epsilon^w - \epsilon_{\theta, G}^w(x_t^w, t, c)\|_2^2 - \|\epsilon^w - \epsilon_{\text{ref}}^w(x_t^w, t, c)\|_2^2 \right) - \left(\|\epsilon^l - \epsilon_{\theta, G}^l(x_t^l, t, c)\|_2^2 - \|\epsilon^l - \epsilon_{\text{ref}}^l(x_t^l, t, c)\|_2^2 \right) \right) \right) \right]$; \triangleleft DPO loss

25 $G \leftarrow G - \eta \frac{\partial \mathcal{L}_{\text{Diff-DPO}}}{\partial G}$; \triangleleft update the weights

26 $\theta \leftarrow \theta + G$; \triangleleft store the LoRA weights into the original model

27 **return** θ

reward in Eq. (16) with the form from Eq. (19):

$$\mathcal{L}_{\text{DPO}}(\theta) = -\mathbb{E}_{x_0^w, x_0^l, c} \left[\log \sigma \left(\beta \left(\log \frac{p_\theta(x_0^w | c)}{p_{\text{ref}}(x_0^w | c)} - \log \frac{p_\theta(x_0^l | c)}{p_{\text{ref}}(x_0^l | c)} \right) \right) \right]. \quad (20)$$

To grasp the intuition behind \mathcal{L}_{DPO} , we can analyze its gradient with respect to θ :

$$\begin{aligned} \frac{\partial \mathcal{L}_{\text{DPO}}(\theta)}{\partial \theta} = & -\beta \cdot \mathbb{E}_{x_0^w, x_0^l, c} \left[\sigma \left(\hat{r}_\theta(x_0^l, c) - \hat{r}_\theta(x_0^w, c) \right) \cdot \right. \\ & \left. \left(\frac{\partial \log p_\theta(x_0^w | c)}{\partial \theta} - \frac{\partial \log p_\theta(x_0^l | c)}{\partial \theta} \right) \right], \end{aligned} \quad (21)$$

with $\hat{r}_\theta(x_0, c) = \beta \cdot \log \frac{p_\theta(x_0 | c)}{p_{\text{ref}}(x_0 | c)}$. By analyzing Eq. (21), as dis-

cussed in [15], it is evident that the DPO objective enhances the likelihood of favored examples, while diminishing it for the unfavored ones. The magnitude of the update is proportional to the error in \hat{r}_θ . Here, the term “error” refers to the degree to which \hat{r}_θ incorrectly prioritizes the sample x_0^l .

6.2 Curriculum-DPO++ for Diffusion Models

We formally present the application of Curriculum-DPO++ to diffusion models in Algorithm 2. The initial steps 1-19, which outline the curriculum strategy, are identical with those used in the implementation for consistency models described in Algorithm 1. Steps 20-24 are changed to include the forward

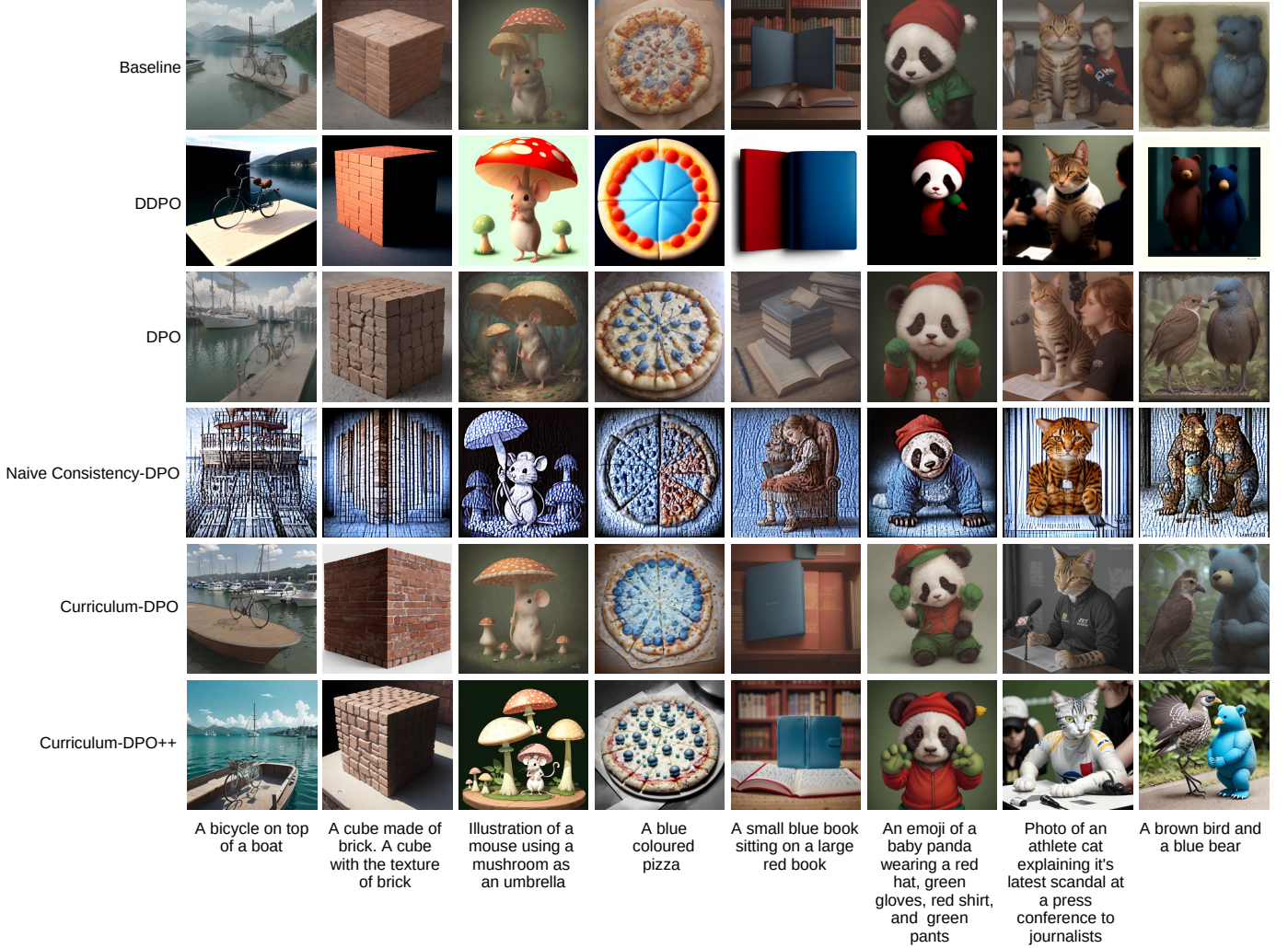


Fig. 8: Qualitative results before and after fine-tuning for the text alignment task on DrawBench. The fine-tuning methods are: DDPO, DPO, Naive Consistency-DPO, Curriculum-DPO, and Curriculum-DPO++. Best viewed in color.

process for the preferred and less preferred samples, along with the Diffusion-DPO loss defined in Eq. (5).

6.3 More Qualitative Results

In Figure 8, we show qualitative results when fine-tuning the model for text alignment on D_2 (DrawBench). In addition to images generated by baselines, DPO, DDPO, Curriculum-DPO and Curriculum-DPO++, we also include images generated by a naive implementation of Consistency-DPO. This implementation refers to the most direct adaptation of Diffusion-DPO to consistency models. More precisely, we substitute the noise estimation in the Diffusion-DPO objective with the consistency distillation loss used in consistency models. However, applying this modification directly breaks the consistency property required by these models and leads to poor results, as illustrated in the 4th row of Figure 8.

In Figures 9 and 10, we present qualitative results after fine-tuning the models with HPSv2 and LAION Aesthetics Predictor as reward models on D_1 , respectively. Fine-tuning for human preference (Figure 9) generally results in generating images with more details for the LCM model. Curriculum-DPO and Curriculum-DPO++ produce better aesthetics for both foreground objects and the background.

For the SD model, Curriculum-DPO and Curriculum-DPO++ exhibit a better alignment with the text prompt, our methods being the only ones able to generate the ant on a bike, as displayed in the last column. Moreover, there are cases where Curriculum-DPO++ synthesizes the animals and the activities more clearly than Curriculum-DPO, as shown in the “squirrel washing the dishes” example. Fine-tuning to improve the visual appeal (Figure 10) translates into better aesthetics for the animals, as expected. However, Curriculum-DPO and Curriculum-DPO++ return several examples that look better than the rest, *e.g.* the camel in the sixth column and the dog in the third column.

6.4 Samples with Masked Prompt Embeddings

In Figure 11, we present examples of images generated while masking the corresponding input prompt embeddings. For each prompt, we showcase samples obtained under different masking ratios. As the masking ratio increases, the generated images progressively degrade, exhibiting reduced alignment with the textual description and a noticeable drop in visual quality, ranging from poorly defined structures to complete noise. The illustrated examples confirm that masking the text embeddings enables the generation of preference pairs with

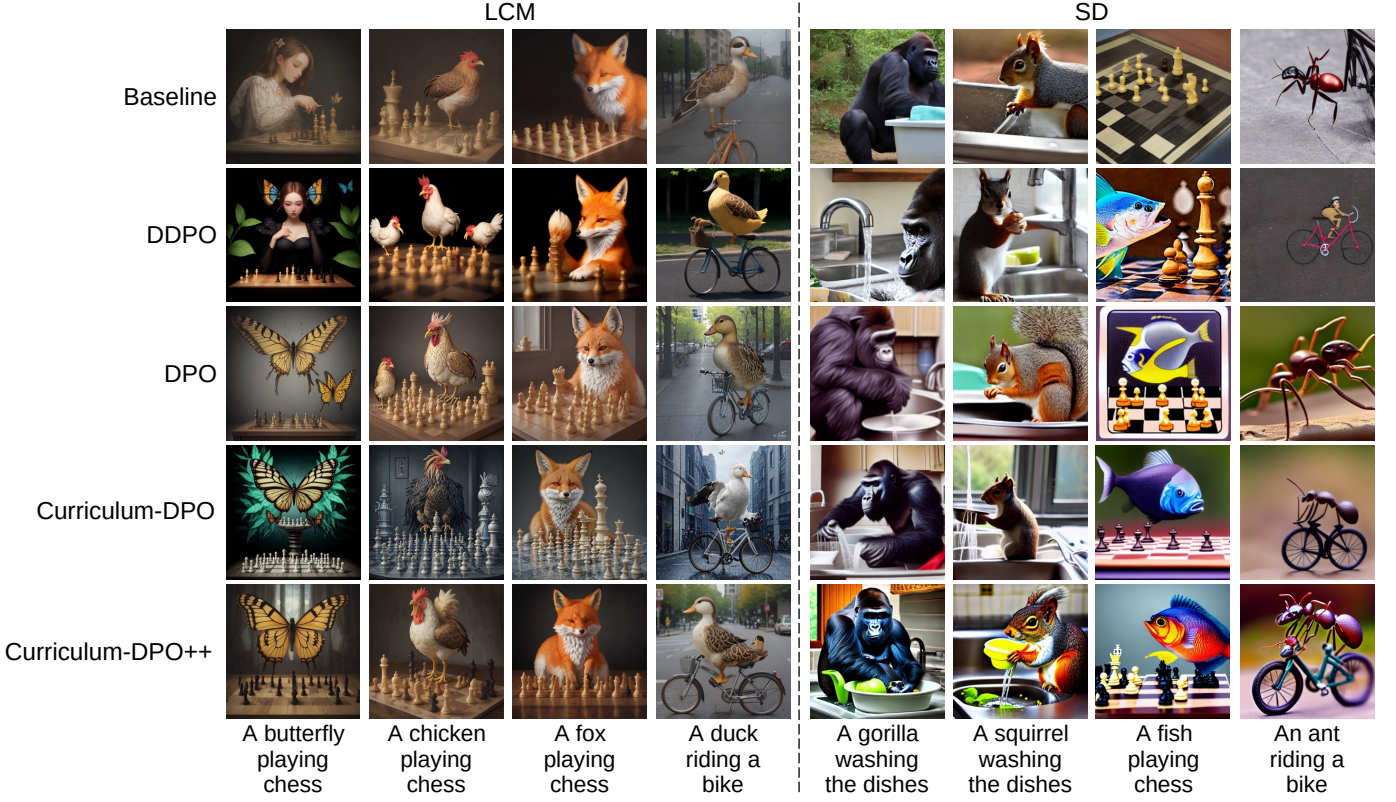


Fig. 9: Qualitative results after fine-tuning with HPSv2 as the reward model (human preference). The fine-tuning alternatives are: DDPO, DPO, Curriculum-DPO, and Curriculum-DPO++. Best viewed in color.

controllable differences between winning and losing examples, without having to use a reward model. By controlling the generation of preference pairs via the masking ratio, we thus obtain a reward-model-free data-level curriculum.

6.5 Limitations

One limitation of our framework is the introduction of additional hyperparameters, such as B or K . These might require tuning in order to find the optimal values, which involves more computing power. This is a downside of curriculum learning [55], which inherently implies the addition of hyperparameters to control the curriculum learning process. Nevertheless, in the ablation study from Section 4, we demonstrate that Curriculum-DPO and Curriculum-DPO++ outperform all baselines for multiple hyperparameter combinations. Therefore, suboptimal hyperparameter choices can still improve the generative models.

A limitation of text-to-image generative models (as well as reward models) is the poor ability to disambiguate words in the input prompt. This can be observed especially in the prompt alignment task, where a word with multiple meanings or connotations leads to generating poor results. For example, the prompt “a turkey washing the dishes” often results in images of a cooked meal instead of a live bird, as depicted in the first column of Figure 12. In the remaining columns, we show a few other failure cases of the LCM baseline and its fine-tuned variants. In the second column, we show that the models fail to understand complex actions, they simply generate a pizza for a prompt that involves the action of paying for one. The examples included in the third column reveal a lack of robustness to misspellings,

and, in the last column, the examples indicate that text generation is only marginally improved. Curriculum learning does not specifically address these limitations of generative and reward models.



Fig. 10: Qualitative results after fine-tuning with the LAION Aesthetics Predictor as the reward model. The fine-tuning alternatives are: DDPO, DPO Curriculum-DPO, and Curriculum-DPO++. Best viewed in color.

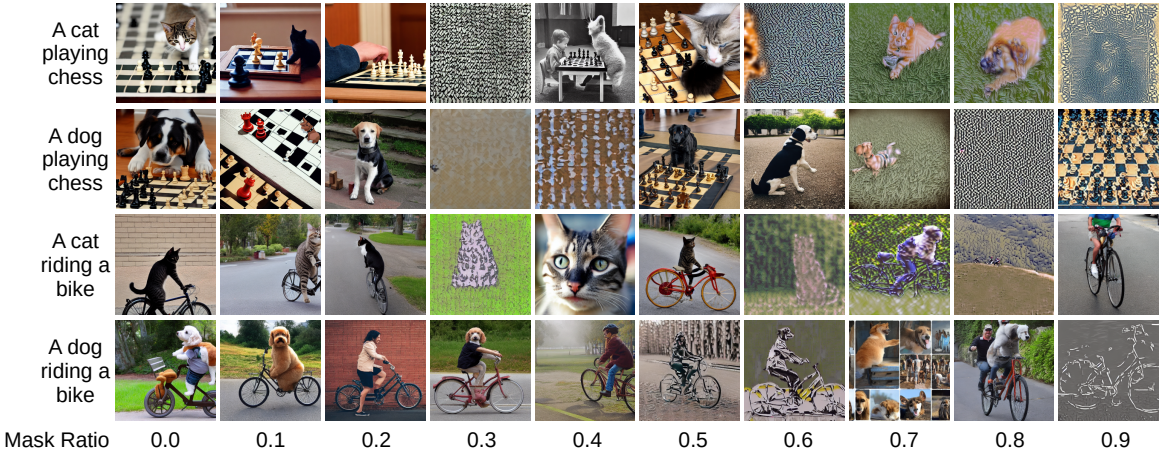


Fig. 11: Samples generated with SDv1.5 that have the prompt embedding masked with a ratio between 0.0 and 0.9. Masking more of the text embeddings leads to lower quality images, enabling a reward-model-free curriculum. Best viewed in color.

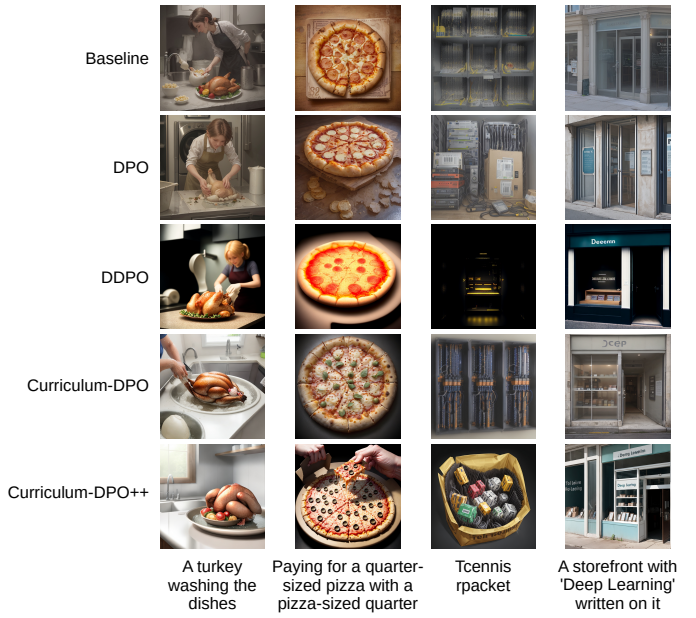


Fig. 12: Failure cases of the LCM baseline and fine-tuned variants. In the first column, the models consistently generate a meal to depict the turkey, instead of a bird. In the second column, the models struggle to understand the prompt, they generate a pizza, but they fail to showcase the action of paying for one. The third column demonstrates that the models are not robust to misspellings, and, in the last column, the models fail to generate the required text.